
Master Thesis

# Multidimensional Analysis of Non-Standard Neutrino Interactions Using the Proposed ESS$\nu$SB Experiment

Fredrik Hansen

Theoretical Particle Physics, Department of Theoretical Physics,
School of Engineering Sciences,
KTH Royal Institute of Technology, SE-106 91 Stockholm, Sweden

Stockholm, Sweden 2015

Typeset in LaTeX

TRITA-FYS 2015:71
ISSN 0280-316X
ISRN KTH/FYS/--15:71--SE


Printed in Sweden by Universitetsservice US AB, Stockholm October 2015

# Abstract

The Standard Model of particle physics contains only massless neutrinos. Observations of neutrino oscillations does however disprove the existence of massless neutrinos. Various models try to describe massive neutrinos and most of these New Physics models cause so-called Non-Standard Interactions. Non-Standard Interactions is a collective term for particle interactions not allowed by the Standard Model.

A simulation of the proposed ESS$\nu$SB experiment with a modified version of the GLoBES software is used to explore the implications of allowing these Non-Standard Interactions. The simulated data are mainly used to predict upper bounds for the new parameters that could be set if the full experiment was performed. All of the Non-Standard Interaction parameters are allowed to be non-zero simultaneously by the usage of an efficient Monte Carlo algorithm.



**Key words**: New Physics, Non-Standard Matter Interactions, Long Baseline Neutrino Experiment, Neutrino CP-Violation, ESS$\nu$SB.



# Sammanfattning

Standardmodellen inom partikelfysik inkluderar endast masslösa neutriner. Massiva neutriner är dock en följd av observationer av fenomenet neutrino-oscillationer. Det finns flera modeller som försöker beskriva denna nya fysik och de flesta av dessa ger upphov till så kallade icke-standard växelverkningar. Icke-standard växelverkningar är ett samlingsnamn för växelverkningar som inte kan förklaras av standardmodellen.

Det föreslagna ESS$\nu$SB experimentet har simulerats med hjälp av en modifierad version av mjukvaran GLoBES för att utforska de implikationer som följer av att introducera icke-standardinteraktioner. Den simulerade datan används i huvudsak för att uppskatta de övre gränser för de nya parametrarna som skulle kunna fastställas om experimentet genomfördes. Alla icke-standardparametrar tillåts vara nollskilda samtidigt med hjälp av en effektiv Monte Carlo algoritm.



**Nyckelord**: Ny fysik, icke-standard växelverkningar, oscillationsexperiment med lång baslinje, neutrino CP-Brott, ESS$\nu$SB.

# Preface

This work has been performed at the Theoretical Particle Physics group at KTH Royal Institute of Technology in Stockholm, Sweden.

I would foremost like thank my supervisors Tommy Ohlsson, Mattias Blennow and Sandhya Choubey for guiding me through this project. The rest of the particle physics group has helped me as well by offering many important insights and a multitude of intriguing lunch discussions. I am especially indebted to Sushant Raut for his assistance in getting my modified version of GLoBES to work properly.

Finally I must thank Erik Holmgren and David Aceituno for proof-reading earlier versions of this report as well as commenting on my work in general throughout the project. David Aceituno should be mentioned an additional time for allowing me to use his efficient Monte Carlo minimiser, which has been used repeatedly throughout the project.

# Contents

# Glossary

| | |
|---|---|
| AEDL | Abstract Experiment Definition Language. |
| AMANDA | Antarctic Muon And Neutrino Detector Array. |
| C.L. | Confidence Level. |
| CC | Charged Current. |
| CNGS | CERN Neutrinos to Gran Sasso. |
| CP | Charge-Parity. |
| DM | Dark Matter. |
| DOF | Degree Of Freedom. |
| DUNE | Deep Underground Neutrino Experiment. |
| ESS | European Spallation Source. |
| ESS$\nu$SB | European Spallation Source Neutrino Super Beam. |
| GLoBES | General Long Baseline Experiment Simulator. |
| ICARUS | Imaging Cosmic And Rare Underground Signals. |
| JUNO | Jiangmen Underground Neutrino Observatory. |
| K2K | KEK to Kamioka. |
| KamLAND | Kamioka Liquid Scintillator Antineutrino Detector. |
| KATRIN | Karlsruhe Tritium Neutrino Experiment. |
| LNV | Lepton Number Violation. |
| MINOS | Main Injector Neutrino Oscillation Search. |
| MSW | Mikheyev–Smirnov–Wolfenstein effect. |
| MUV | Minimal Unitarity Violation. |
| NC | Neutral Current. |
| NF | Neutrino Factory. |
| NO$\nu$A | NuMI Off-Axis $\nu_e$ Appearance. |
| NSI | Non-Standard Interaction. |
| OPERA | Oscillation Project with Emulsion-tRacking Apparatus. |
| PDG | Particle Data Group. |
| PMNS | Pontecorvo-Maki-Nakagawa-Sakata matrix. |
| POT | Protons On Target. |

| | |
|---|---|
| QFT | Quantum Field Theory. |
| QM | Quantum Mechanics. |
| RENO | Reactor Experiment for Neutrino Oscillations. |
| SBL | Short Baseline. |
| SK | Super Kamiokande. |
| SM | Standard Model. |
| T2K | Tokai to Kamioka. |
| WDM | Warm Dark Matter. |

# Chapter 1

# Introduction

The field of physics is in general divided into the two categories of classical and modern physics. What is now known as classical physics was for a long time the only known branch and is mainly focused around classical mechanics, classical electrodynamics and classical thermodynamics. Modern physics on the other hand contains all theories describing systems that are not limited by large length scales and low velocities.

The first modern theory which is in some sense the basis for all further modern physics is the theory of Quantum Mechanics (QM). The theory arose from the descriptions of black-body radiation by Max Planck and the photoelectric effect by Albert Einstein in the early 20th century. QM is valid at small length scales and at low velocities.

The second group of fundamental theories for the modern approach to physics is that of special and general relativity also formulated by Albert Einstein. The theory makes it possible to describe systems with motions close to the speed of light.

The third and final group of modern theories is that of Quantum Field Theory (QFT). The theory combines the small length scales of QM with the high velocities of relativity in order to describe particle interactions at high energies.

Particle physics is a branch of physics that was initially based on the ancient Greek concept that there should be some fundamental building block that all larger bodies are constructed from. Some early attempts at finding these fundamental particles lead to the discovery of the atom. Particle physics was at the time purely classical. The discovery of the first currently accepted fundamental particle was made in the late 19th century. Soon after this the atomic structure was explored by Ernest Rutherford's gold foil experiment. Throughout the 20th century QM, the theory of relativity and QFT were developed and combined with classical particle physics to form what is now known as high-energy particle physics.

Of all models which are based on the theories particle physics the Standard Model (SM) is the most successful. It is a model that describe the interactions

of a collection of fundamental particles. The SM proposes twelve fermions, four types of gauge bosons and the Higgs particle. The gauge bosons do according to the SM allow the fermions to couple to each other. These interactions lead to certain predictions for physical observables which in general are consistent with experimental observations.

The basis for the model was the combination of the theories of electromagnetism and weak interactions into a single framework known as the electroweak interaction [1]. Later works incorporated the Higgs mechanism [2, 3] into the SM framework [4]. The Higgs mechanism is predicted to be the source for the masses of the gauge bosons while the fermions acquire mass indirectly by Yukawa interaction with the Higgs field. Due to helicity of neutrinos in the SM no mass is given to them from the Higgs mechanism.

In 1957 Bruno Pontecorvo proposed the ground-breaking new theory that the flavour of the neutrino, the particle with the lowest mass in the SM, oscillated as the particle propagated through space [5]. Pontecorvo's theory was based on the basic principles of quantum mechanics. In 1968 Pontecorvo once again published an article on the subject where he initially came to the conclusion that the neutrino and antineutrino of a particular flavour are two distinct particles [6]. He did at this point compare flavour to other known conserved properties such as strangeness. At the time there were several experiments verifying these theoretical arguments of Pontecorvo. The lack of detection of double beta decay for $^{48}Ca$ is one of the principle reasons why conservation of flavour was assumed. Another issue raised by Pontecorvo in his 1968 paper was the issue of the so-called solar neutrino problem.

The solar neutrino problem is a discrepancy between the detected amount of electron neutrinos originating from the sun and the expected amount predicted by the Standard Solar Model. The first observation of this discrepancy was performed by Davis, Harmer and Hoffman in 1968 [7]. They found that there was a deficit in the electron neutrino flux from the Sun. In order to explain this discrepancy other undetected neutrino flavours were introduced into the the solar neutrino flux. The justification of these added flavours was that neutrinos would oscillate due to a non-zero mass according to the predictions of Pontecorvo [8] and subsequently explain the observed deficit. This major discovery was awarded part of the 2002 Nobel Prize in physics.

Even though the SM mostly describe the neutrino effects it is not completely satisfactory. The most important attribute which is completely overlooked by the SM is that neutrinos have an experimentally observed mass and subsequent flavour mixing. The 2015 Nobel Prize in physics was awarded jointly to Takaaki Kajita and Arthur B. McDonald for the discovery of neutrino oscillations. In order to describe this phenomenon extensions of the SM must be used in high-precision measurements. Most of these extensions do however enable Non-Standard Interactions (NSIs) by default [9]. NSIs belong to a collection of effective couplings that are not described by the SM. An important scientific challenge in high-energy particle physics is to limit these NSI effects in order to justify the SM framework used so far or in the case of the presence of NSIs refute the SM.

This thesis has the purpose to investigate NSIs and specifically the case of matter interactions in the proposed European Spallation Source Neutrino Super Beam (ESS$\nu$SB) experiment. Some established tools such as the GLoBES software will be used in order to simplify the numerical calculations. The topic of NSIs is a specialised topic within particle physics and a certain understanding of particle physics in general and in particular a deep understanding of analytical mechanics and quantum mechanics is required. In addition some basic knowledge in the field of statistical analysis is assumed.

This thesis first discuss standard neutrino oscillations in Chapter 2 and non-standard neutrino oscillations in Chapter 3. Chapters 4 and 5 then continue to present important neutrino experiments which have been and could be central for our understanding of Nature. In Chapter 6 the simulations performed as part of this project are presented. Finally conclusions that can be drawn from the simulated data are summarised in Chapter 7.

# Chapter 2

# Standard Neutrino Oscillations

Chapter 2 is a summary of the physics behind standard neutrino oscillations. Even though the massive neutrinos cannot be describe by the Standard Model it is possible to explain neutrino oscillations in terms of Standard Model interactions. The chapter covers three flavour oscillations both in vacuum and in matter. Finally the chapter explains some basic concepts regarding CP violation.

## 2.1 Flavour Mixing

The flavour eigenstates of the neutrinos are assumed not to be equal to the mass eigenstates but rather a linear combination of them in order to account for flavour nonconserving phenomena of experiments described in Refs. [7, 8, 10]. The transformation from mass eigenstates to flavour eigenstates is on the form of a general unitary rotation in three dimensions. A general $n \times n$ unitary matrix can be described by $n(n-1)/2$ angles and $n(n+1)/2$ phases. In the case of $n = 3$ this will result in 3 angles and 6 phases. However 5 of the phases only contribute to the overall phase of the matrix and the flavour eigenstates and will subsequently not be of interest as the oscillation probabilities will only be dependent on the absolute value of the operator. A representation of the general mixing matrix is

$$U = \begin{pmatrix} c_{12}c_{13} & s_{12}c_{13} & s_{13}e^{-i\delta_{CP}} \\ -s_{12}c_{23} - c_{12}s_{23}s_{13}e^{i\delta_{CP}} & c_{12}c_{23} - s_{12}s_{23}s_{13}e^{i\delta_{CP}} & s_{23}c_{13} \\ s_{12}s_{23} - c_{12}c_{23}s_{13}e^{i\delta_{CP}} & -c_{12}s_{23} - s_{12}c_{23}s_{13}e^{i\delta_{CP}} & c_{23}c_{13} \end{pmatrix}, \quad (2.1)$$

where $s_{ij}$ and $c_{ij}$ are abbreviation of $\sin(\theta_{ij})$ and $\cos(\theta_{ij})$, $\theta_{ij}$ being the mixing angles and $\delta_{CP}$ is the only remaining phase [11]. This matrix is commonly known

as the Pontecorvo–Maki–Nakagawa–Sakata (PMNS) matrix. The relation between the flavour basis and the mass basis can thus be described by

$$|\nu_\alpha\rangle = \sum_j U^*_{\alpha j} |\nu_j\rangle \,, \tag{2.2}$$

where $\alpha$ is a flavour state and $j$ is a mass state. In the remainder of this thesis Greek letters will denote flavour states and Roman letters will denote mass states.

## 2.2 Time Evolution

The general time evolution of the neutrino flavour states is simply given by

$$|\nu_\alpha(t)\rangle = e^{-iHt} |\nu_\alpha\rangle \,. \tag{2.3}$$

The flavour states are separate from the eigenstates of the Hamiltonian and calculations are greatly simplified by making the transformation to the mass basis as in Equation 2.2 when doing the time evolution. The mass eigenstates are the eigenstates of the Hamiltonian and therefore $e^{-iHt} |\nu_j\rangle = e^{-iE_j t} |\nu_j\rangle$. By performing this transformation the expression for the time evolution in terms of the mass basis is

$$e^{-iHt} |\nu_\alpha\rangle = \sum_{\alpha'} |\nu_{\alpha'}\rangle \sum_j U_{\alpha' j} e^{-iE_j t} U^*_{\alpha j}. \tag{2.4}$$

## 2.3 Oscillation Probability

As the state of the neutrino is given by $|\nu_\alpha(t)\rangle$ the probability to find the neutrino in state $\beta$ at time $t$ is given by $P(\nu_\alpha \to \nu_\beta; t) = |\langle \nu_\beta | \nu_\alpha(t)\rangle|^2$. By combining this with the high energy limit of $E_j = \sqrt{p^2 + m_j^2} \approx p + \frac{m_j^2}{2E}$ it can be found that

$$\begin{aligned} P(\nu_\alpha \to \nu_\beta; t) = |\langle \nu_\beta | \nu_\alpha(t)\rangle|^2 &= \left| \langle \nu_\beta | \sum_{\alpha'} |\nu_{\alpha'}\rangle \sum_j U_{\alpha' j} e^{-i\left(p + \frac{m_j^2}{2E}\right)t} U^*_{\alpha j} \right|^2 \\ &= \left| \sum_j U_{\beta j} e^{-i\left(p + \frac{m_j^2}{2E}\right)t} U^*_{\alpha j} \right|^2 = \left| \sum_j U_{\beta j} e^{-i\frac{m_j^2}{2E}t} U^*_{\alpha j} \right|^2 . \end{aligned} \tag{2.5}$$

The removal of the phase $p$ in the final step is due to the fact that an overall phase does not influence the absolute value of a complex number. Equation 2.5 can be

simplified by various assumptions. A common assumption is to only include two-flavour oscillations and thus only letting $j$ sum over two states. In the case of the two-flavour oscillation $\nu_e \to \nu_\mu$ where the flavour mixing is given by

$$U = \begin{pmatrix} \cos\theta & \sin\theta \\ -\sin\theta & \cos\theta \end{pmatrix}. \tag{2.6}$$

In the specific case of $P(\nu_e \to \nu_\mu; t)$, Equation 2.5 simplifies to

$$\begin{aligned} P(\nu_e \to \nu_\mu; t) = |\langle \nu_\mu | \nu_e(t) \rangle|^2 &= \left| U_{\mu 1} e^{-i\frac{m_1^2}{2E}t} U_{e1}^* + U_{\mu 2} e^{-i\frac{m_2^2}{2E}t} U_{e2}^* \right|^2 \\ &= \left| sce^{i\frac{\left(m_1^2 - m_2^2\right)}{4E}t} - sce^{-i\frac{\left(m_1^2 - m_2^2\right)}{4E}t} \right|^2 \left| e^{-i\frac{\left(m_1^2 + m_2^2\right)}{4E}t} \right|^2 \\ &= \sin^2(2\theta) \sin^2\left(\frac{\Delta m_{21}^2}{4E} t\right), \end{aligned} \tag{2.7}$$

where $s = \sin\theta$, $c = \cos\theta$ and $\Delta m_{21}^2 = m_2^2 - m_1^2$. At this point it is very clear that the probability to find that the electron neutrino has become a muon neutrino at time $t$ oscillates with respect to time in the case of massive neutrinos. In the case that the neutrino would be massless ($m_i = 0$) there would be no oscillations as $\Delta m_{ij}^2 = 0$.

Equation 2.5 can also be simplified in the three-flavour neutrino scenario so that the oscillatory attributes are apparent, this is done as follows

$$\begin{aligned} P(\nu_\alpha \to \nu_\beta; t) &= \sum_{j,k} U_{\beta j} U_{\alpha j}^* U_{\beta k}^* U_{\alpha k} \left( e^{-i\frac{(m_j^2 - m_k^2)}{2E}t} - 1 + 1 \right) \\ &= \sum_{j,k} U_{\beta j} U_{\alpha j}^* U_{\beta k}^* U_{\alpha k} - \sum_{j,k} U_{\beta j} U_{\alpha j}^* U_{\beta k}^* U_{\alpha k} \left( 1 - e^{-i\frac{\Delta m_{jk}^2}{2E}t} \right) \\ &= \delta_{\alpha\beta} - 2\sum_{j>k} Re(U_{\beta j} U_{\alpha j}^* U_{\beta k}^* U_{\alpha k}) Re\left( 1 - e^{-i\frac{\Delta m_{jk}^2}{2E}t} \right) \\ &+ 2\sum_{j>k} Im(U_{\beta j} U_{\alpha j}^* U_{\beta k}^* U_{\alpha k}) Im\left( 1 - e^{-i\frac{\Delta m_{jk}^2}{2E}t} \right) \\ &= \delta_{\alpha\beta} - 4\sum_{j>k} Re(U_{\beta j} U_{\alpha j}^* U_{\beta k}^* U_{\alpha k}) \sin^2\left( \frac{\Delta m_{jk}^2}{4E} t \right) \\ &+ 2\sum_{j>k} Im(U_{\beta j} U_{\alpha j}^* U_{\beta k}^* U_{\alpha k}) \sin\left( \frac{\Delta m_{jk}^2}{2E} t \right) \end{aligned} \tag{2.8}$$

where $\delta_{\alpha\beta}$ is the Kronecker delta. It should be emphasised that $\delta_{\alpha\beta}$ will throughout the rest of this work be used for the phase of a complex parameter rather than for the Kronecker delta.

## 2.4 Standard Neutrino Interactions in Matter

When including standard matter interactions the necessary modifications are to include Charged Currents (CC) and Neutral Currents (NC) into the Hamiltonian of the system. By making this inclusion the new Hamiltonian is given by

$$H_{SM} = U \begin{pmatrix} E_1 & 0 & 0 \\ 0 & E_2 & 0 \\ 0 & 0 & E_3 \end{pmatrix} U^\dagger + \begin{pmatrix} V_{CC} & 0 & 0 \\ 0 & 0 & 0 \\ 0 & 0 & 0 \end{pmatrix} + \begin{pmatrix} V_{NC} & 0 & 0 \\ 0 & V_{NC} & 0 \\ 0 & 0 & V_{NC} \end{pmatrix}. \quad (2.9)$$

As can be seen in Equation 2.3 a contribution to the Hamiltonian proportional to the identity will only influence the overall phase of the time evolution; any terms proportional to identity can be subtracted without changing the probability. In this case it would simplify calculations to subtract $H'_{SM} = H_{SM} - (E_1 + V_{NC})\mathbb{1}$. This new Hamiltonian will from now on be called $H$ as it is the most convenient way of describing the system

$$H_{SM} = \frac{1}{2E} U \begin{pmatrix} 0 & 0 & 0 \\ 0 & \Delta m^2_{21} & 0 \\ 0 & 0 & \Delta m^2_{31} \end{pmatrix} U^\dagger + \begin{pmatrix} V_{CC} & 0 & 0 \\ 0 & 0 & 0 \\ 0 & 0 & 0 \end{pmatrix}. \quad (2.10)$$

where the high-energy limit of $E_j \approx p + \frac{m_j^2}{2E}$ has once again been used. Notice at this point that if $U$ and $V_{CC}$ are real $H_{SM}$ must be real as well.

The result of matter interactions is thus that the mass eigenstates and eigenvalues (of the Hamiltonian) become dependent on the matter density. This means that the flavour evolution has to be integrated over the density of matter along the path of the neutrino. The addition of SM matter interaction makes it inconvenient to determine the probability analytically but it can however be calculated numerically by software such as GLoBES [12, 13].

A simple way of dealing with this problem would be to consider the matter interactions as a small perturbation of the stable state of $UE_iU^\dagger$. This can be done by changing the basis of $V_{CC}$ in Equation 2.10 from the flavour basis to the vacuum mass basis as

$$H_{SM} = V_{CC} U \begin{pmatrix} c_{12}^2 c_{13}^2 & s_{12} c_{12} c_{13}^2 & c_{12} s_{13} c_{13} e^{-i\delta_{CP}} \\ s_{12} c_{12} c_{13}^2 & s_{12}^2 c_{13}^2 + \frac{\Delta m^2_{21}}{2EV_{CC}} & s_{12} s_{13} c_{13} e^{-i\delta_{CP}} \\ c_{12} s_{13} c_{13} e^{i\delta_{CP}} & s_{12} s_{13} c_{13} e^{i\delta_{CP}} & s_{13}^2 + \frac{\Delta m^2_{31}}{2EV_{CC}} \end{pmatrix} U^\dagger. \quad (2.11)$$

By then making the approximation $s_{13} \approx 0$ and $c_{13} \approx 1$, Equation 2.11 can be significantly simplified. This would correspond to expanding the matrix in terms

of $\theta_{13}$ and only keeping the first term

$$H_{SM} \approx V_{CC} U \begin{pmatrix} c_{12}^2 & s_{12}c_{12} & 0 \\ s_{12}c_{12} & s_{12}^2 + \frac{\Delta m_{21}^2}{2EV_{CC}} & 0 \\ 0 & 0 & \frac{\Delta m_{31}^2}{2EV_{CC}} \end{pmatrix} U^\dagger. \tag{2.12}$$

This expression can be diagonalised by a simple rotation around the third axis $R_3(\phi)$ and the separation of another phase such that

$$H_{SM} \approx \frac{1}{2E} U R_3(\phi) \begin{pmatrix} 0 & 0 & 0 \\ 0 & \Delta\widetilde{m}_{21}^2 & 0 \\ 0 & 0 & \Delta\widetilde{m}_{31}^2 \end{pmatrix} R_3(-\phi) U^\dagger, \tag{2.13}$$

where

$$\begin{aligned} \tan(2\phi) &\approx \frac{\sin(2\theta_{12})}{\left[\cos(2\theta_{12}) - \frac{\Delta m_{12}^2}{2EV_{CC}}\right]}, \\ \Delta\widetilde{m}_{21}^2 &\approx V_{CC}\left(\frac{\Delta m_{21}^2 - 2\Delta m_{31}^2}{2V_{CC}} + E - \sqrt{-\frac{E\Delta m_{21}^2}{V_{CC}}\cos(2\theta_{12}) + \frac{\Delta m_{21}^4}{4V_{CC}^2} + E^2}\right), \\ \Delta\widetilde{m}_{31}^2 &\approx V_{CC}\left(\frac{\Delta m_{21}^2 - 2\Delta m_{31}^2}{2V_{CC}} + E + \sqrt{-\frac{E\Delta m_{21}^2}{V_{CC}}\cos(2\theta_{12}) + \frac{\Delta m_{21}^4}{4V_{CC}^2} + E^2}\right). \end{aligned} \tag{2.14}$$

From this, the conclusion that both the eigenvalues and the eigenbasis of the Hamiltonian are very dependent on $V_{CC}$ in the case of matter interactions.

Calculating the total rotation around the third axis caused by $U$ and $R_3(\phi)$ as $\theta'_{12} = \theta_{12} + \phi$ the matter resonance can be investigated. The oscillation amplitude will attain a maximum at a certain matter density and is now known as the Mikheyev–Smirnov–Wolfenstein (MSW) effect [14, 15]. The MSW resonance will be at the point where the rotation $\sin(\theta'_{12})$ is at a maximum and $\tan(2\theta'_{12})$ will go towards infinity at this point

$$\begin{aligned} \tan(2\theta'_{12}) = \tan(2\theta_{12} + 2\phi) &= \frac{\tan(2\theta_{12}) + \tan(2\phi)}{1 - \tan(2\theta_{12})\tan(2\phi)} \\ &= \frac{\sin(4\theta_{12}) - \frac{\Delta m_{21}^2}{2EV_{CC}}\sin(2\theta_{12})}{\cos(4\theta_{12}) - \frac{\Delta m_{21}^2}{2EV_{CC}}\cos(2\theta_{12})}. \end{aligned} \tag{2.15}$$

This equation thus determines the resonance density as $V_{CC} = \frac{\Delta m_{21}^2}{2E}\frac{\cos(2\theta_{12})}{\cos(4\theta_{12})}$. It should be noted that the matter interaction Hamiltonian in general is dependent on the spatial coordinate of the particle by the intermediate dependence on the matter density $V_{CC}$. In the case of constant density the rotation of Equation 2.13 will simply be a fixed rotation. It must however be noted that $s_{13} \approx 0$ and $c_{13} \approx 1$ has recently become a less accurate approximation since $\theta_{13}$ has been found to be larger than expected by the Daya Bay experiment [16].

## 2.5 Hamiltonian Formalism

The simple vacuum oscillations presented earlier in Chapter 2 could be described by the new potentially flavour changing propagator seen in Figure 2.1. This is the only possible propagation caused by the Hamiltonian

$$H_{SM} = \frac{1}{2E} U \begin{pmatrix} 0 & 0 & 0 \\ 0 & \Delta m^2_{21} & 0 \\ 0 & 0 & \Delta m^2_{31} \end{pmatrix} U^\dagger. \tag{2.16}$$


**Figure 2.1:** Potentially flavour violating propagator. Neutrino oscillations result from neutrinos having a non-zero mass.

By introducing the matter interactions as in Equation 2.9, the additional interaction vertices due to the Charged Current (CC) and Neutral Current (NC) are shown in Figure 2.2.

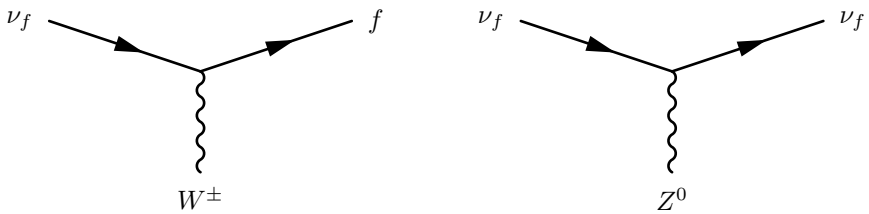


**Figure 2.2:** Feynman diagrams of SM neutrino vertices. The left diagram illustrates neutrino flavour-conserving charged interaction and the right illustrates neutrino flavour-conserving neutral interaction. Note that neutrinos interact only via the weak interaction and that gravity is ignored throughout this work.

When introducing matter interaction Equation 2.3 is no longer completely true as the matter density parameter $V_{CC}$ in general can depend on the position and therefore also on time. The correct expression for the time evolution of the flavour states in this case will be

$$|\nu_\alpha(t)\rangle = e^{-i\int_0^t H dt'} |\nu_\alpha(0)\rangle\,. \tag{2.17}$$

Obviously this expression becomes Equation 2.3 when the Hamiltonian is independent of time. Equation 2.17 is in general very difficult to solve analytically

when the Hamiltonian is time-dependent. The equation can however be solved numerically without much trouble.

## 2.6 CP, T and CPT Conservation in Vacuum

CP conservation in the case of neutrino oscillations corresponds to the charge-parity conjugation $|\langle\nu_\beta|\nu_\alpha(t)\rangle|^2 \to |\langle\bar{\nu}_\beta|\bar{\nu}_\alpha(t)\rangle|^2$. By inserting the vacuum expression for the flavour states it can be seen that the transformation corresponds to

$$\left|\sum_j U_{\beta j} e^{-iE_j t} U^*_{\alpha j}\right|^2 \to \left|\sum_j U^*_{\beta j} e^{-iE_j t} U_{\alpha j}\right|^2 . \tag{2.18}$$

CP is thus clearly conserved while $U_{\alpha j} = U^*_{\alpha j}$ as all elements of $U$ are scalars and thus commute with all other elements. The only CP violating parameter in the extension for massive neutrinos of the SM theory is $\delta_{CP}$ which only conserves CP under the condition $\delta_{CP} = n\pi$ where $n$ is an integer. By introducing the CC matter interactions the expression does become more complicated and the only simple solution for CP conservation is the condition $\delta_{CP} = 0$.

T conservation concerns what effect changing the sign of the time has on the oscillation probability. If the probability does not change when performing the transform $|\langle\nu_\beta|\nu_\alpha(t)\rangle|^2 \to |\langle\nu_\beta|\nu_\alpha(-t)\rangle|^2$, T is said to be conserved. This transform is completely equivalent to switching the initial and final flavours as can be seen by

$$\begin{aligned}\left|\sum_j U_{\beta j} e^{-iE_j t} U^*_{\alpha j}\right|^2 \to \left|\sum_j U_{\beta j} e^{+iE_j t} U^*_{\alpha j}\right|^2 &= \left|\left(\sum_j U_{\alpha j} e^{-iE_j t} U^*_{\beta j}\right)^*\right|^2 \\ &= \left|\sum_j U_{\alpha j} e^{-iE_j t} U^*_{\beta j}\right|^2 .\end{aligned} \tag{2.19}$$

The condition of Equation 2.19 is equivalent to that of Equation 2.18 due to the unitarity of $U$. Thus $U_{\alpha j} = U^*_{\alpha j}$ would imply both CP and T conservation while $U_{\alpha j} \neq U^*_{\alpha j}$ means the presence of both CP and T violation.

Extending these transformations to CPT the overall result is the condition $U_{\alpha j} = \left(U^*_{\alpha j}\right)^*$ which must be true. CPT is thus always conserved in standard neutrino oscillations while CP and T can simultaneously be violated by non-zero values for $\delta_{CP}$.

### 2.6.1 CP Asymmetry in Vacuum

The CP asymmetry is calculated by the formula in Equation 2.20 and is a measure of the asymmetry between particles and anti-particle in a certain process

$$A_{\alpha\beta} = \frac{P_{\alpha\beta} - P_{\bar{\alpha}\bar{\beta}}}{P_{\alpha\beta} + P_{\bar{\alpha}\bar{\beta}}} \tag{2.20}$$

The asymmetry as a function of oscillation length in vacuum for each initial and final flavour combination can be seen Figure 2.3. In the case of the initial electron flavour the asymmetry from $\nu_e \to \nu_\mu$ has equal amplitude but opposite sign compared to that from $\nu_e \to \nu_\tau$. This means that the overall asymmetry will cancel if the probabilities of these oscillations are equal. In the case of the initial muon and tau flavour these two contributions will not cancel and an overall CP violation will be present. If initial muons and taus are present in equal numbers, the partial contributions from the two oscillations will cancel. Notice that the disappearance channel $\nu_\alpha \to \nu_\alpha$ never cause CP violation in vacuum.

The parameter $\delta_{CP}$ could thus cause local CP violation, where local signifies CP violation in certain flavour oscillations. If equal numbers of $\nu_\mu$ and $\nu_\tau$ are present, the total violation for all oscillations will be zero. Our framework does however include matter interactions which could cause global CP violation, where global violation is characterarised by a total violation after adding the local violations from the three flavours. This is signified by total CP violation even if equal numbers of $\nu_\mu$ and $\nu_\tau$ are considered. This global CP violation is a result of the matter-antimatter asymmetry in the universe.

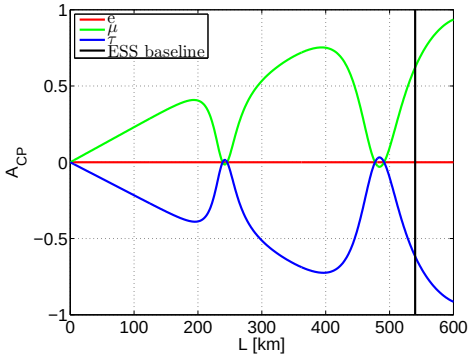


**(a)** Initial $\nu_e$

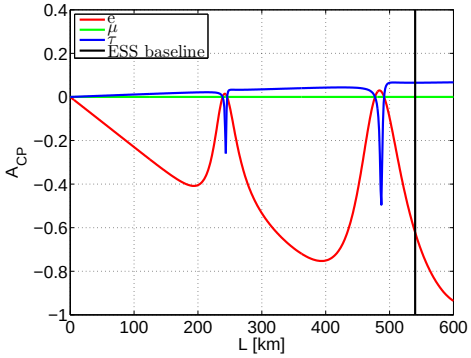


**(b)** Initial $\nu_\mu$

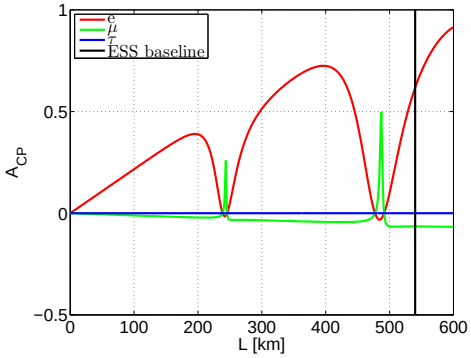


**(c)** Initial $\nu_\tau$

**Figure 2.3:** $A_{\alpha\beta}$ with different initial flavour. Red means CP asymmetry caused by oscillation into $\nu_e$, green into $\nu_\mu$ and blue into $\nu_\tau$. The black line represents the baseline of the ESS$\nu$SB experiment. All standard parameters were set to the best fit from Ref. [11].

# Chapter 3

# Non-Standard Neutrino Interactions

There are many models for different physics beyond the Standard Model. Several of them have an origin in the unexplained mass of neutrinos which is a clear indication that the SM is not enough to describe the fundamental laws of Nature. A common implication of these New Physics models are the Non-Standard matter Interactions. This chapter covers some results caused by the introduction of NSI parameters as well as some different approaches to these new interactions. The chapter also contains a brief summary on the CP implications of NSIs.

## 3.1 Hamiltonian Formalism

By including NSIs there must be a modification of the effective Lagrangian representing the new interaction vertices. The NSI Lagrangian then takes the form [17]

$$\mathcal{L}_{NSI} = -2\sqrt{2}\varepsilon_{\alpha\beta}^{ff'P} G_F(\bar{\nu}_\alpha \gamma_\mu P_L \nu_\beta)(\bar{f}\gamma^\mu P f'), \tag{3.1}$$

where $f$ and $f'$ are fermions which the neutrinos interact with. Electrons, $u$ quarks and $d$ quarks are the only fermions existing in any significant numbers in the universe according to current understanding of it and the other fermions are subsequently ignored. Here $G_f$ is the Fermi coupling constant, $\gamma_\mu$ is one of the gamma matrices and $P$ is either of the projection operators $P_L = (1-\gamma_5)/2$ or $P_R = (1+\gamma_5)/2$. By making the rough approximation that the number of electrons, protons and neutrons are the same on Earth the ansatz $\varepsilon_{\alpha\beta} = \sum_P (\varepsilon_{\alpha\beta}^{eeP} + 3\varepsilon_{\alpha\beta}^{uuP} + 3\varepsilon_{\alpha\beta}^{ddP})$ can be made. With this new set of parameters we can draw the new NSI Feynman diagrams in Figure 3.1.

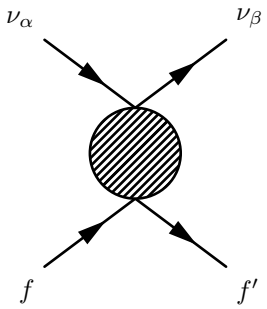


**Figure 3.1:** Effective Feynman diagram of dimension $d = 6$ NSI neutrino vertex. The vertex respresent an effective interaction between two neutrinos and two fermions. Flavour is not necessarily conserved in this NSI vertex.

## 3.2 Non-Standard Neutrino Interactions in Matter

In order to include all possible interactions in the model we add a new interaction term to the Hamiltonian. This new term will represent interactions that are generally not allowed in the Standard Model. In the case of NSIs the new term will be similar to the regular SM matter interactions. The most general hermitian matrix representing Non-Standard matter Interactions is

$$H_{NSI} = A \begin{pmatrix} \varepsilon_{ee} & \varepsilon_{e\mu} & \varepsilon_{e\tau} \\ \varepsilon^*_{e\mu} & \varepsilon_{\mu\mu} & \varepsilon_{\mu\tau} \\ \varepsilon^*_{e\tau} & \varepsilon^*_{\mu\tau} & \varepsilon_{\tau\tau} \end{pmatrix}, \tag{3.2}$$

where the $\varepsilon_{\alpha\beta} = |\varepsilon_{\alpha\beta}|e^{i\delta_{\alpha\beta}}$ are complex parameters and $A = \sqrt{2}G_F N_e$ just as in the case of standard matter interactions [9]. The Non-Standard Hamiltonian $H_{NSI}$ should be added to $H_{SM}$ to form an effective Hamiltonian

$$H_{eff} = H_{SM} + H_{NSI}. \tag{3.3}$$

The effective Hamiltonian $H_{eff}$ is the operator that would correspond to the observable energy in an experiment. Subsequently, as $H_{NSI}$ could be expected to be small compared to $H_{SM}$ it could be considered a small perturbation from the latter.

## 3.3 Oscillation Experiment Parameter Sensitivity

A neutrino oscillation experiment will only be sensitive to the probability to oscillate or not and does not depend on the phase of the neutrino state. In principle, for oscillation experiments, $A\varepsilon_{\alpha\alpha}\mathbb{1}$ can be subtract from the Hamiltonian which become independent of the parameter $\varepsilon_{\alpha\alpha}$. Such a separation would correspond to separating a phase in the probability as can be seen in

$$\begin{aligned} P(\nu_\alpha \to \nu_\beta; t) &= \left| e^{-i\int (H_{SM}+H_{NSI})dt} \right|^2 = \left| e^{-i\int (H_{SM}+H_{NSI})dt} \right|^2 \left| e^{i\int A\varepsilon_{\mu\mu}\mathbb{1}dt} \right|^2 \\ &= \left| e^{-i\int (H_{SM}+H_{NSI}-A\varepsilon_{\mu\mu}\mathbb{1})dt} \right|^2 . \end{aligned} \tag{3.4}$$

It should be noted that the same procedure is done for the regular oscillation parameters in SM oscillations when the two mass differences $\Delta m^2_{ij}$ are considered rather than all three masses $m^2_i$. The choice of which parameter to remove is arbitrary as the same argument is valid for any of the three diagonal elements. The choice in this case was based on the existing bounds on the NSI parameters where the upper bound on $\varepsilon_{\mu\mu}$ from Ref. [17] is significantly stronger than those on $\varepsilon_{ee}$ and $\varepsilon_{\tau\tau}$. By then subtracting $\varepsilon_{\mu\mu}$ the remaining parameters will almost correspond to the old parameters if $\varepsilon_{\mu\mu}$ is significantly smaller than the other diagonal elements. The only effect of $\varepsilon_{\mu\mu}$ not being significantly smaller than the other parameters is that the bounds from this framework will not compare to the bounds from Ref. [17].

The relation between all three diagonal parameters is discussed in Chapter 6 and is illustrated in Figure 6.6. Subsequently the true values of all three parameter bounds could be increased simultaneously while still being self-consistent. This is a manifestation of the inherent lack of sensitivity towards all six parameters NSI parameters in neutrino oscillation experiments. The only other relation where this effect has a significant contribution is the relation between $\varepsilon_{e\mu}$ and $\varepsilon_{e\tau}$. This is however an isolated phenomenon and does not allow for large self-consistent upper bounds.

We now rename $(H_{NSI}-\varepsilon_{\mu\mu}\mathbb{1}) \to H_{NSI}$, $(\varepsilon_{ee}-\varepsilon_{\mu\mu}) \to \varepsilon_{ee}$ and $(\varepsilon_{\tau\tau}-\varepsilon_{\mu\mu}) \to \varepsilon_{\tau\tau}$ in order to produce a convenient formalism. It must be emphasised that the new version of $\varepsilon_{\alpha\beta}$ will have upper bounds that cannot be directly compared to the upper bounds of the old parameters

$$H_{NSI} = A \begin{pmatrix} \varepsilon_{ee} & \varepsilon_{e\mu} & \varepsilon_{e\tau} \\ \varepsilon^*_{e\mu} & 0 & \varepsilon_{\mu\tau} \\ \varepsilon^*_{e\tau} & \varepsilon^*_{\mu\tau} & \varepsilon_{\tau\tau} \end{pmatrix}, \tag{3.5}$$

where $H_{NSI}$ is fully described by five parameters rather than six parameters. The old parameter $\varepsilon_{\mu\mu}$ will obviously affect the physical state of the neutrino in respect to what phase it has but will not be visible in the experimental data of any neutrino oscillation experiment. For example we could add a NC interaction of any strength to the Hamiltonian without changing the oscillation probability.

## 3.4 Majorana Type NSI Phases

The true nature of the neutrino is not known and it can either be a particle of Dirac or Majorana type. Dirac particles are not its own antiparticle while Majorana particles are. Neutrinoless double beta decay has for some time been the only viable experiment in order to determine if neutrinos are particles of the Majorana or the Dirac type. A major difficulty in determining the nature of neutrinos by this way is the fact that a signal from Majorana neutrinos is difficult to distinguish from a signal originating from another source such as right-handed currents, heavy right-handed neutrinos, leptoquark-Higgs couplings, compositeness and supersymmetric particle exchange [18].

Majorana phases are two phases that must be added to $H_{SM}$ if the neutrino is found to be a Majorana particle. The phases have the form seen in

$$U \to U \begin{pmatrix} e^{i\rho} & 0 & 0 \\ 0 & e^{i\sigma} & 0 \\ 0 & 0 & 1 \end{pmatrix}. \tag{3.6}$$

and would be caused by a modified mass term in the Lagrangian. The new term is a manifestation of the Weinberg operator ($d = 5$) and would be on the form $m_\nu \bar{\nu}_L^C \nu_L$. Oscillation experiments would in general not be sensitive to these new Majorana phases as opposed to the Dirac phase ($\delta_{CP}$). The experiments that would be sensitive to the Majorana phases would be any experiment containing Lepton Number Violating (LNV) processes such as in neutrinoless double beta decay [19].

In order to limit the scope of this thesis to a certain area of research Majorana phases will not be considered in the simulations of Chapter 6. They are obviously of interest in the case of New Physics outside of the SM but due to their lack of influence on oscillation probabilities they can safely be ignored in neutrino oscillation experiments.

The effective Hamiltonian from Equation 3.3 could be parametrised by an effective set of parameters

$$H_{eff} = \frac{1}{2E} \widetilde{U} \begin{pmatrix} 0 & 0 & 0 \\ 0 & \Delta\widetilde{m}^2_{21} & 0 \\ 0 & 0 & \Delta\widetilde{m}^2_{31} \end{pmatrix} \widetilde{U}^\dagger. \tag{3.7}$$

This expression has 8 Degrees of Freedom (DOF) where 5 DOF are regular parameters, 1 DOF is the Dirac phase and 2 DOF are the Majorana phases. By then fixing the standard parameters in the model for NSIs is becomes clear that the NSI parameter set of 8 parameters has 8 DOF of which the 3 NSI phases incorporate the Dirac DOF as well as the two Majorana DOF. As a neutrino oscillation experiments are not sensitive to the 2 Majorana DOF there cannot be any multidimensional bounds on the NSI phases and these must be marginalised over $2\pi$.

In general two of the phases in the NSI model are of Majorana type. In order to simplify the calculations these values are minimised over in all simulations. This is

easily done because there is an obvious periodic dependence on $\delta_{\alpha\beta}$. The fact that the NSI phase of Dirac type is ignored does not inhibit the evaluation of the NSI parameters as the $\delta_{CP}$ degree of freedom is still considered. The only direct result of ignoring the Dirac NSI phase is that the value for $\delta_{CP}$ will not be very accurate.

## 3.5 CP, T and CPT Conservation in Matter

When including complex NSI parameters $\delta_{CP}$ will no longer be the only source of CP-violation in the Hamiltonian. Each new off-diagonal element on the form $|\varepsilon_{\alpha\beta}|e^{i\delta_{\alpha\beta}}$ will contain an independent CP violating parameter $\delta_{\alpha\beta}$.

The only situation which can be fully explored is the case of matter interaction in the case of constant matter density throughout the full experiment. By adding the NSI Hamiltonian in Equation 3.5 to the SM Hamiltonian and then diagonalising it and subtracting a phase the resulting probability can be described as

$$P(\nu_\alpha \to \nu_\beta; t) = \left| \sum_j \widetilde{U}_{\beta j}(A) e^{-i\widetilde{E}_j(A)t} \widetilde{U}^*_{\alpha j}(A) \right|^2 . \tag{3.8}$$

By then making the same transforms as in Equations 2.18 and 2.19 it will be obvious that the condition that must be fulfilled for CP or T invariance is $\widetilde{U}_{\alpha j} = \widetilde{U}^*_{\alpha j}$. This condition will always be fulfilled in the case of $\delta_{CP} = m\pi$ and $\delta_{\alpha\beta} = n\pi$ where $m$ and $n$ are integers. It is however more difficult to find general properties of the more complex situations where matter density is not constant. In order to draw any real conclusions from this an explicit expression for $\widetilde{U}_{\alpha j}$ is needed. Such an expression would however in the case of varying matter density be very complex due to the dependence on $A$.

### 3.5.1 CP Asymmetry in Matter

CP violation can be divided into two main categories; genuine CP violation due to the nature of the propagating neutrinos and fake CP violation caused by matter interactions [20]. The matter interaction is called a fake contribution to CP violation due to fact that the asymmetry is caused by an unexplained asymmetry in matter density. Genuine CP violation such as the ones caused by NSIs could indirectly affect the matter asymmetry. NSIs are therefore an important area of research as it potentially could explain the long-standing problem of the matter-antimatter asymmetry in the universe.

Explicit calculations of the oscillation probabilities up to $\mathcal{O}(|\varepsilon|)$ at short distances and under the assumption of CP conservation are performed in Ref. [20]. In the SM case

$$A^{SM}_{CP} \approx -\Delta m^2_{21} \frac{L}{2E} \mathrm{Im}\left( \frac{U_{e2} U^*_{\mu 2}}{U_{e3} U^*_{\mu 3}} \right). \tag{3.9}$$

is found to be the lowest order term in a Taylor expansion. In the case of new physics on the other hand

$$A_{CP}^{NP} \approx \begin{cases} -\dfrac{4E}{\Delta m_{31}^2 L}\mathrm{Im}\left(\dfrac{\varepsilon_{\mu e}^{d*}+\varepsilon_{e\mu}^{s}}{U_{e3}U_{\mu 3}^{*}}\right), \text{ large } s_{13} \\ -\dfrac{4E}{\Delta m_{21}^2 L}\mathrm{Im}\left(\dfrac{\varepsilon_{\mu e}^{d*}+\varepsilon_{e\mu}^{s}}{U_{e2}U_{\mu 2}^{*}}\right), \text{ small } s_{13} \end{cases} \tag{3.10}$$

is found to be the leading term. It should be noted that in general CP violation is suppressed by the small mixing angles of the PMNS matrix and subsequently that observations of CP violations could be a strong indication of NSIs [20].

## 3.6 Source and Detector NSIs

Another prominent NSI model is that of source and detector NSIs. These are characterised by the assumption that producing a neutrino of a certain flavour at a certain source will result in a superposition of that flavour state and the other flavours. The same is assumed for detectors but in general the detector states can be different from the source states. It gives rise to the so-called zero distance effect meaning that we could have a detector positioned at the distance 0 from the source that detects a neutrino of another flavour than the one produced [9]. The source and detector NSIs are on the form

$$\begin{aligned} |\nu_\alpha^s\rangle &= |\nu_\alpha\rangle + \sum_\beta \varepsilon_{\alpha\beta}^s |\nu_\beta\rangle = (1+\varepsilon^s)U|\nu_j\rangle\,, \\ \langle\nu_\beta^d| &= \langle\nu_\beta| + \sum_\alpha \varepsilon_{\alpha\beta}^d \langle\nu_\alpha| = \langle\nu_j| U^\dagger[1+(\varepsilon^d)^\dagger]. \end{aligned} \tag{3.11}$$

Introducing source and detector NSIs is equivalent to the statement that the produced and detected neutrinos are not of the flavours $e$, $\mu$, $\tau$ but rather $e_s$, $\mu_s$, $\tau_s$ and $e_d$, $\mu_d$, $\tau_d$. If $\varepsilon_s = \varepsilon_d$ we can simply call these new flavours $e$, $\mu$, $\tau$ and have the same interactions as before introducing these parameters. Thus source and detector NSIs are only of interest if $\varepsilon_s \neq \varepsilon_d$ where the interaction Hamiltonian can be written as

$$H_{NSI}^{sd} = \frac{(1+\varepsilon^d)U\Delta U^\dagger[1+(\varepsilon^s)^\dagger]}{|1+\varepsilon^d||1+(\varepsilon^s)^\dagger|}. \tag{3.12}$$

By transforming the Hamiltonian from the $|\nu_\alpha\rangle$ space to the $|\nu_\alpha^s\rangle$ space Equation 3.12 becomes

$$H_{NSI}^{sd} = \frac{[1+(\varepsilon^s)^\dagger](1+\varepsilon^d)U\Delta U^\dagger}{|1+\varepsilon^d||1+(\varepsilon^s)^\dagger|}, \tag{3.13}$$

where it is clear that the case $\varepsilon^s = \varepsilon^d$ is trivial. The fact that the Hamiltonian for source and detector NSIs is simply a linear transform of the regular vacuum

Hamiltonian can be observed in Equation 3.13. This has a very clear physical interpretation as introducing source and detector NSIs is equivalent with the idea that the Hamiltonian contains the transform from the source flavour basis to the detector flavour basis in addition to the regular oscillatory terms. This could be the case for example if the flavour of a neutrino was gauge dependent.

## 3.7 Unitarity of the PMNS Matrix

Some New Physics scenarios enable non-unitarity of the neutrino mixing matrix. The condition required for the mixing matrix to be non-unitary is that the Hamiltonian is not Hermitian due to a degeneracy in the eigenvalues. According to Ref. [21] a non-Hermitian Hamiltonian could be constructed in a coherent QM theory as long as there is a PT symmetry to compensate.

The most prominent theory of non-unitarity in neutrino physics is the Minimal Unitarity Violation (MUV) scheme which contains the assumptions that non-unitarity is allowed in the neutrino terms of the three flavour SM Lagrangian. The MUV scheme does produce zero distance (or source and detector) effects. By refraining from using the hermiticity assumption oscillation experiments will not be able to determine all the mixing parameters and decay experiments must be used to complement the oscillation experiments [22].

Physical attributes that are sensitive to the MUV scheme include the weak mixing angle, the $Z$ and $W$ decay processes and the $W$ boson mass and must all be appropriately modified in order to incorporate the MUV scheme. The observations of these constants could also be compared to theoretical predictions in order to detect upper bounds of the MUV parameters [23].

Due to the strong bounds on the oscillation parameters in the case of exclusively SM interactions [11] there is no room for degenerate eigenvalues in the mass eigenbasis. The conclusion that can be drawn from this is that unitarity violating Hamiltonians are only allowed in a New Physics scenario where the current bounds are not as strong. The simulations performed in this work are performed using the assumption of the Hamiltonian being Hermitian. The MUV scheme is nonetheless an intriguing approach to New Physics in neutrino oscillations.

## 3.8 Sterile Neutrinos

The concept of sterile neutrinos is used for neutrinos that do not interact by any other means than by gravity. Such neutrino models are generally characterised by the sterile neutrinos being right-handed neutrinos. The number of sterile neutrinos is difficult to estimate due to no present experiment being sensitive to the gravitational pull on the relevant energy scales. Sterile neutrinos could contribute to the Lagrangian with either a Dirac or a Majorana mass term [24].

The existence of sterile neutrinos could in theory mean that sterile neutrinos are the main constituents of dark matter (DM). Sterile neutrinos do not interact by the weak force and are subsequently a relevant DM candidate due to them being very long-lived. It is a so-called Warm Dark Matter (WDM) candidate. Using bounds on DM particles certain constraints concerning stability, radiative decay and structural formation could be imposed on sterile neutrinos. If sterile neutrinos would only be a contributing factor to DM the constraints would weaken significantly [24].

Sterile neutrinos will not be considered in the simulations of this work.

# Chapter 4

# Past, Present and Future Neutrino Experiments

This chapter contains a brief overview of past and present neutrino experiments that have been important for our understanding of neutrino physics. In addition a few future and conceptual experiments are discussed.

## 4.1 Past Neutrino Experiments

It was not until the Super Kamiokande (SK) results of 1998 that precise observations of neutrino oscillations were available. At this point flavour oscillations for atmospheric neutrinos were implied at a significant Confidence Level (C.L.) [10]. Except for monitoring atmospheric and solar neutrinos the SK observatory was built to look for proton decay and supernovae as well as to make measurements in neutrino beam experiments such as K2K and T2K. The structure of SK is that of a large cylindrical water tank buried 1 km underground and containing 50 kilotons ultra pure water. When a neutrino interacts with the water in the tank a particle is produced that could exceed the speed of light in water and thus produce an optical equivalent to a shock wave. The shock wave can then be detected as a ring pattern by the optical detectors along the walls of the tank. This is known as Cherenkov radiation and has been used as the main method of detecting neutrinos [25].

IceCube and its predecessor AMANDA are other innovative neutrino observatories positioned on Antarctica and consisting of a large number of photomultiplier tubes drilled far into the ice. They were constructed to search for point sources of high energy neutrinos, indirect searches for dark matter, supernovae and sterile neutrinos [26].

There has been a series of neutrino experiments utilising the production of neutrinos in a nuclear reactor. Examples of these experiments are KamLAND [27],

RENO [28], Double Chooz [29] and Daya Bay [30]. The KamLAND detector absorbs neutrinos by 1 kiloton ultra-pure liquid scintillator suspended by a transparent nylon balloon in non-scintillating oil. The balloon is monitored by photomultiplier tubes on a spherical stainless steel vessel. The detector is surrounded by 53 nuclear reactors which are considered in the analysis of the data. KamLAND was able to produce the most precise measurements of the 2-neutrino oscillation model parameter $\Delta m^2$ [27]. At the time the KamLAND experiment produced measurements at unpreceeded precision which since then have been adapted for the 3-neutrino oscillation model. The Daya Bay experiment was also very successful and detected an unexpectedly large value for the parameter $\theta_{13}$ in 2012 [16].

The final source for a neutrino experiment is that of a neutrino beam. The beam is generally produced at an accelerator and then directed towards a certain detector. MINOS uses the NuMI beam produced at Fermilab to analyse oscillations [31]. The CNGS beam is a neutrino beam produced at CERN and aimed towards Gran Sasso. Both the OPERA and the ICARUS experiments use this beam to test neutrino attributes. T2K is a continuation of the K2K long baseline neutrino oscillation experiment using a neutrino beam produced at the J-PARC facility [32].

### 4.1.1 SM Parameter Values

A requirement of neutrino oscillations is that the neutrinos are massive so that there is a mass difference between the different mass eigenstates. The mass difference between eigenstates are represented by $\Delta m^2_{ij}$ and constitute two of the SM neutrino oscillation parameters. The standard oscillation parameters $\Delta m^2_{21}$ and $\theta_{12}$ are currently most accurately determined by a fit using KamLAND, global solar neutrino, short baseline (SBL) reactor and accelerator data. The mass difference $|\Delta m^2_{32}|$ is on the other hand found from a fit of T2K, MINOS and Daya Bay data. The mixing angle $\theta_{23}$ is most accurately determined by the T2K experiment and $\theta_{13}$ can be found from the average of Daya Bay, Double Chooz and RENO data [11]. The remaining parameter $\delta_{CP}$ is currently barely constrained at all. This parameterisation is made to find a simple description of neutrino oscillation in vacuum as a function of the parameters.

## 4.2 Future Neutrino Experiments

Most future neutrino experiments are designed to detect the remaining unknown SM parameters i.e. $\text{sgn}(\Delta m^2_{31})$, $\delta_{CP}$, the absolute mass scale and the Majorana CP-violating phases. Neutrino oscillation experiments could in principle determine $\text{sgn}(\Delta m^2_{31})$ and $\delta_{CP}$ while neutrinoless double beta decay experiments could determine the Majorana or Dirac nature of neutrinos and the absolute mass scale could be found by $\beta$-decay experiments [9].

Many of the future neutrino experiments are based on the success of present and past experiments. Among others are NO$\nu$A [33], JUNO [34] and DUNE [35].

Some of the new experiments propose approaches to the determination of physical parameters which have not been explored before. KATRIN is for example a neutrino experiment designed to find the absolute mass scale of neutrinos with a sub-eV precision. A direct measurement of the neutrino mass scale could be of importance in the dark matter question and in determining if the neutrino is a Dirac or Majorana particle [36].

The ESS$\nu$SB experiment is a promising proposed neutrino oscillation experiment which could be sensitive to several of the unknown parameters. ESS$\nu$SB is proposed to be an extension of the ESS neutron beam facility which currently is under construction. This experiment will be studied in detail in Chapter 5.

Most of these future experiments have potential to further our understanding of neutrino oscillations by improving existing bounds on parameters as well as to measure new bounds on unobserved parameters.

### 4.2.1 Neutrino Factory

There are conceptual designs for a neutrino beam going straight through the Earth called a Neutrino Factory (NF). These could in principle be very sensitive to all of the oscillation parameters and most importantly to large $\theta_{13}$ and NSIs. The experiment would consist of three major parts. First there would be a particle accelerator complex accelerating particles to high energies. These particles are then sent towards a target where pions are produced. The pions will then be directed towards a neutrino detector on the other side of the Earth so that a significant number of the resulting neutrinos from pion decay ends up at the detector. The target presents a substantial engineering challenge as it must be able to dissipate the excess energy from a high energy particle beam. Feasibility of NFs are continuously being evaluated [37].

# Chapter 5

# European Spallation Source Neutrino Super Beam

Chapter 5 is mostly based on the study [38] which proposes a neutrino super beam to be constructed at the future ESS facility. This beam will enable various important oscillation experiments. The proposal has been used as a guideline both for presenting the technical specifications in this chapter but also for defining the simulation parameters in Chapter 6.

## 5.1 Experimental Equipment

The European Spallation Source (ESS) in Lund, Sweden will be a high power proton ($H^+$) linac which will start to produce neutrons at the target in 2019. The equipment will be fully functional in 2022. The neutron beam produced by the ESS facility is intended to be used both in research and industry. The site is currently under construction and is expected to have significant scientific impact. The proton linac will be 500 m long and produce $2.7 \times 10^{23}$ POT $\mathrm{yr}^{-1}$ (Protons On Target) at 2 GeV energy when completed.

### 5.1.1 Neutrino Beam

Among the proposed uses for the ESS proton linac is the production of the so-called ESS Neutrino Super Beam (ESS$\nu$SB) experiment. The protons will be ejected in 14 pulses each second of 2.86 ms length and 62.5 mA current. After the proton pulse hits a target, the resulting pions are forced into a 20 m long decay tunnel. 20 m is long enough for a significant amount of particles to decay into a muon-muon neutrino pair. The decay tunnel is however not long enough for the muons to then decay into electrons.

A proton pulse consists of $1.1 \times 10^{15}$ protons and is accelerated to 2 GeV. When the facility is fully operational in 2022 the protons are supposed to be accelerated to energies as high as 3 GeV. Most of the resulting neutrinos are in the 200-500 MeV energy range with a mean of 300 MeV. The experimental data used in the simulation do however rather imply a mean closer to 250 MeV.

According to estimates in Ref. [38], the signal can be assumed to have a 5 % systematic error and the background can be assumed to have a 10 % systematic error. These assumptions will be used in the simulations but would not significantly change the results if proven optimistic. The experiment is proposed to include 2 years of neutrino running and 8 years of antineutrino running.

### 5.1.2 Target Station

When the proton beam reaches the rotating tungsten target various hadrons such as neutrons will form. The main function of ESS is to produce a slow neutron beam which will be used both in research and industry. The target could consist of a packed bed of titanium spheres cooled by helium gas to simplify the cooling process.

Short-lived mesons are produced as the protons hit the target. The most commonly produced meson is the pion which decays into a muon and a muon neutrino in the process $p + p \rightarrow p + n + \pi^+$. The complete decay process of $\pi^+$ is shown in Figure 5.1. The target station also contains a magnetic horn which focuses a set of pions towards the detector. The decay tunnel is another part which is long enough to allow most of the mesons to decay but not long enough to allow a significant number of muons to decay. There has been a proposal of four targets each equipped with a magnetic horn practically cutting the incident power in four from 5 MW to 1.25 MW. The aim of this proposal is to reduce the detriment effects from intense particle bombardment.

The neutrinos produced in pion decay will travel in almost the same direction as the pion. By focusing the pions, the direction of the resulting neutrino beam will be almost the same. The horn is supposed to increase the number of neutrinos with the correct direction with a factor 7.4.

Engineering obstacles that must be overcome in order to complete the ESS$\nu$SB project are for example that the high pulse rate of 14 Hz and the radiation from the intense proton beam could significantly limit the time the equipment can be active. In order to sequentially operate each of the four horns the current pulse generator would have to operate at frequency 56 Hz. The required current at 56 Hz would be 350 kA. There has been a study proving the feasibility of the generator but there is currently no existing generator able to produce the specified pulses. There is also a theory that the beam could cause vibrations in the spheres and subsequently a degradation in the quality of the spheres at the contact points. Its validity is to be evaluated at CERN.

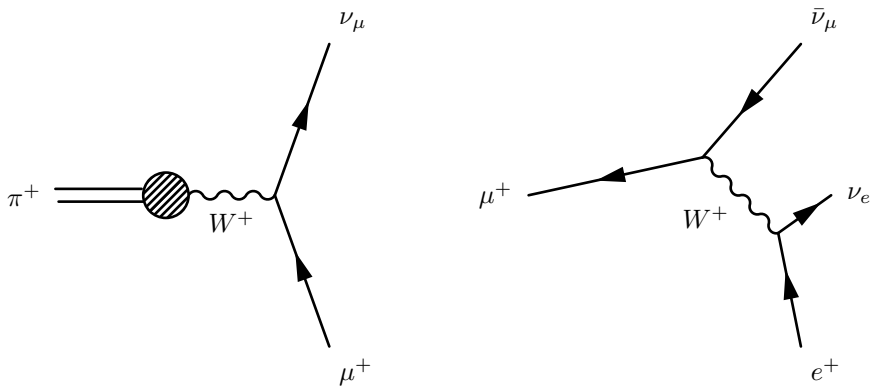


**Figure 5.1:** The pion decay does take place in a so-called decay tunnel. The tunnel must be long enough for a significant number of pions to have decayed into muons but short enough for the next step in the decay chain to not have taken place. The left diagram illustrates the $\pi^-$ decay, while the right diagram illustrates the $\mu^-$ decay. It should be noted that the relative proportions of the three flavours of neutrinos from this decay chain initially is (1:2:0).

### 5.1.3 Detector

The second main component of the proposed experiment is a MEMPHYS-type detector that is going to be placed in a deep mine at a distance of 300-600 km corresponding to the second neutrino oscillation maximum [38]. By positioning the detector close to the maximum the sensitivity of the experiment can be optimised as the appearance channel of the MEMPHYS detector is $\nu_\mu \rightarrow \nu_e$. The detector itself will have a fiducial mass of 500 kt.

The proton beam will be aimed at the chosen detector site. The main alternatives for detector sites are Zinkgruvan at baseline 360 km and Garpenberg at baseline 540 km. The latter would require less excavation while the first has slightly better chances to detect CP violations according to the preliminary simulations. Flavour oscillations in the case of the Garpenberg alternative are illustrated in Figure 5.2.

The probable choice for the mine is the northern Garpenberg mine being situated at the distance of 540 km from the ESS site. The depth of the mine is 830 m. The mine is positioned in a limestone and dolomite rock syncline. The syncline is however surrounded by a granite layer which is suitable for the extensive caverns necessary to house the large MEMPHYS-type detector ($6 \times 10^5$ m$^3$).

A Water Cherenkov detector with a detection threshold lower than 10 MeV could in addition to specifically detecting neutrinos from the ESS$\nu$SB also detect neutrinos from cosmological sources such as supernovae. Such events does make it possible to study oscillation characteristics on length scales of order $10^{17}$ km and time scales of $10^5$ yrs. There are estimates of ESS$\nu$SB being able to detect approx-

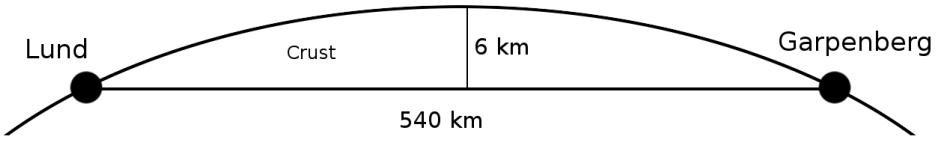


**Figure 5.2:** Illustration of the ESS$\nu$SB neutrino oscillation experiment. The neutrinos will be sent through the Earth crust at a maximum depth of approximately 6 km. This will mean that the matter density will be larger than that of vacuum but approximately constant.

imately $5 \times 10^4$ events from galactic stellar collapses during 10 years of operation [38]. This is possible due to the depth of the proposed mines shields the detector from cosmic ray background radiation. Furthermore the MEMPHYS detector would be able to put a lower limit on the proton lifetime of $10^{35}$ yrs after ten years of collecting data [38].

## 5.2 ESS$\nu$SB Modifications

In order for ESS to be able to produce neutrinos a few modifications of the equipment will be necessary. The addition of the magnetic horn must be in such a way that it is able to focus the produced hadrons. Focusing the currently 2.86 ms long proton pulse will cause heat dissipation problems and is most conveniently solved by making the pulse shorter. The pulse can be reduced to a few µs by the means of multiturn injection. For example 1.5 µs could be achieved by multiturn injection into a 426 m circumference accumulator ring where the particle is accelerated to 94.67 % of the speed of light. To achieve the 1.5 µs pulse the gathered protons are simply ejected in one turn.

The linac must also be able to produce $H^-$ pulses in addition to $H^+$ pulses. The 71.4 ms window between the $H^+$ pulses could be used for this purpose by raising linac pulse frequency from 14 Hz to 28 Hz. Furthermore the average power has to be doubled from 5 MW to 10 MW. This would be the greatest individual cost of the modification and could either be done at the construction of ESS or at a later stage.

### 5.2.1 Accumulator Ring

The purpose of an accumulator ring would be to decrease the length of the pulses. Initially the $H^+$ pulses are 2.86 ms long but by injecting the particles into an accumulator ring which is shorter than the distance travelled during the pulse

length the actual distribution of particles will be folded into multiple turns. When these particles then are ejected from the ring the pulse length will have decreased. The most beneficial pulse length for the neutron peak flux is around 100 µs which requires a ring of about 28 km circumference. An accumulator ring of such large circumference would not be economically viable.

The accumulator ring required for a 1.5 µs pulse length is however much more realistic at 426 m circumference. It should be noted that by decreasing the circumference of the ring the strength of magnetic field keeping the particles in the accelerator must be increased.

## 5.3 Prospects

By these modifications ESS will be able to produce a high intensity neutrino beam without impairing its capacity to produce slow neutrons. Simulations imply that with these specifications significant improvements can be made in both observed SM and NSI neutrino oscillation parameters. These improvements will be further investigated in Chapter 6.

Reference [38] states that about 50 % of the CP phase range can be excluded at $5\sigma$ C.L. for baselines 300-550 km. This would be a significant improvement from our current knowledge as no part of the CP phase range has been excluded so far.

The neutrino mass hierarchy could for ESS$\nu$SB be determined at $3\sigma$ C.L. within a major part of the CP phase range at both considered baselines. The Garpenberg alternative would benefit more from increased beam energy than the Zinkgruvan alternative.

In addition ESS$\nu$SB might be able to improve the bounds on the NSI parameters. This would be of importance in determining the validity of the currently adopted values of the oscillation parameters. Some investigations [39] have been performed to evaluate the sensitivity to source and detector NSIs and the conclusion is that ESS$\nu$SB should be able to improve current bounds.

# Chapter 6

# Simulation of ESS$\nu$SB

GLoBES has been used to make a numerical analysis of the prospects of the ESS$\nu$SB experiment. Chapter 6 contains mainly such a numerical analysis. A new multi-dimensional method for determining the upper bounds for the NSI parameters has been used.

## 6.1 GLoBES

General Long Baseline Experiment Simulator (GLoBES) is a simulation software used to simulate data from long-baseline neutrino oscillation experiments. It can be used to simulate both the point source of neutrinos and a detector of choice. GLoBES is however not able to simulate a spatially extended distribution of sources such as neutrinos from the Sun or from the atmosphere. The experiment is defined in an Abstract Experiment Definition Language (AEDL) file that can be fully customised. The main feature of the software is full incorporation of correlations and degeneracies in the oscillation parameter space [12, 13].

In order to incorporate NSIs the GLoBES software was modified. The modifications consisted mainly of adding the interaction Hamiltonian from Equation 3.2 to that of the existing SM Hamiltonian.

### 6.1.1 Simulation Parameters

GLoBES uses a set of true values for the oscillation parameters. These correspond to what parameter values are assumed in order to decide what the probability to achieve a certain best fit in the parameter space from the experimental data. The true SM parameters were chosen as the currently best-fit values from the PDG particle listings [11]. The CP violating phase $\delta_{CP}$ was set to a non-zero value in order to not unnecessarily suppress CP-violating effects. It was however marginalised over the full $2\pi$ range when determining the upper bounds for the

parameters. The true NSI parameters were all assumed to be zero in the simulations of this chapter unless otherwise stated. We will later explore what results non-zero true values of the NSI parameters would have on the bounds found from the simulation data.

| | |
|---|---|
| $\sin^2(2\theta_{12})$ | 0.846 |
| $\sin^2(2\theta_{23})$ | 0.999 |
| $\sin^2(2\theta_{13})$ | 0.093 |
| $\delta_{CP}$ | $\pi/2$ |
| $\Delta m^2_{21}$ | $7.53 \times 10^{-5}\,\mathrm{eV}^2$ |
| $\Delta m^2_{32}$ | $2.52 \times 10^{-3}\,\mathrm{eV}^2$ |

**Table 6.1:** Choice of true parameter values in GLoBES simulations. These values were used throughout this work if nothing else is stated in the particular case. The values were found in Ref. [11].

The assumed true SM oscillation parameter values are in some sense not very accurate in the case of non-zero NSIs. The PDG values were developed under the assumption of no NSIs and could be subject to change if a significant NSI signal would be found [40]. The scope of this Master thesis can however not incorporate the complications arising from such alterations.

### 6.1.2 Experiment Definition

The AEDL file used by the GLoBES software was constructed by using information found in Ref. [38] concerning the actual experimental setup. For technical specifications on the detector Ref. [41] was consulted. The built-in function of GLoBES for reconstructing neutrino energies due to neutral currents and misidentified neutrinos was found to be inadequate for the relevant energy levels. In order to compensate for this the more accurate migration matrices of Ref. [41] were implemented. A graphical representation of the migration matrices can be seen in Figure 6.1.

In order to find the overall normalisation factor previous simulations were used. By plotting the energy distribution and then making a best fit with the distribution of another simulation [38] the overall normalisation factor was found to be approximately $2.21 \times 10^{-29}$ for the neutrino flux file and $5.63 \times 10^{-30}$ for the antineutrino flux file. The simulated energy distribution can be seen in Figure 6.2.

The appearance and disappearance channels were simulated for the ESSνSB setup. 20 energy bins were used between 0 GeV and 2 GeV. The density is assumed constant at the depth of ESSνSB.

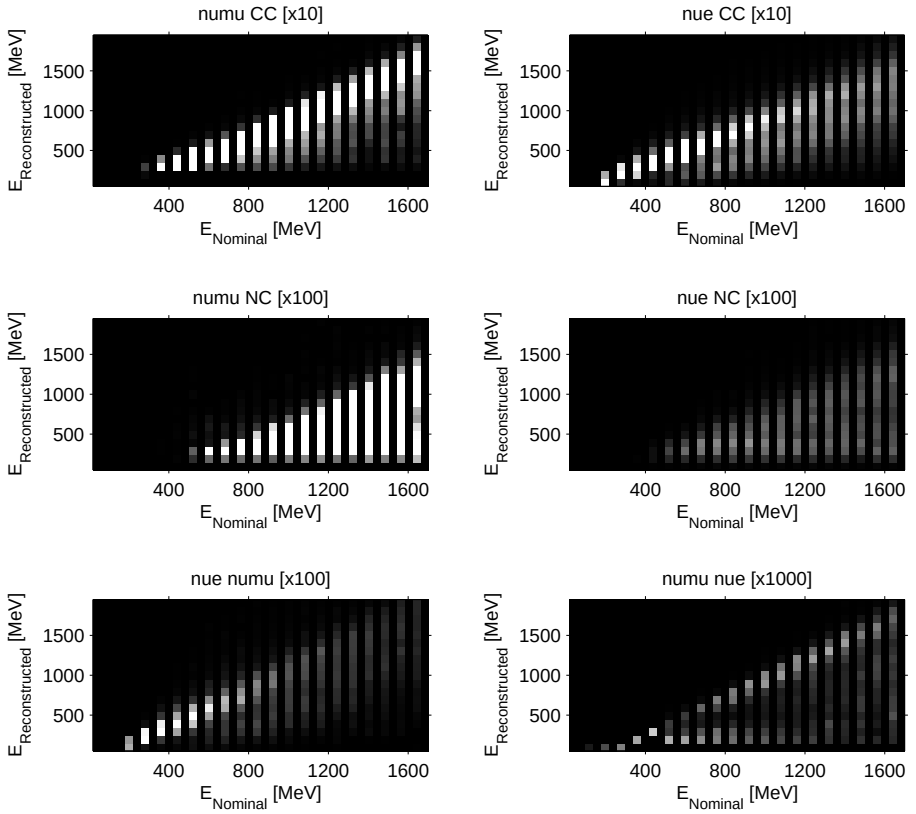


**Figure 6.1:** Migration matrices describe the reconstructed neutrino energy $E_{Reconstructed}$ as a function of the nominal energy $E_{Nominal}$. The magnification ([x10], [x100] or [x1000]) was used on the full migration matrices in order for the non-zero elements to be visible in the illustration. As can be seen the Cherenkov detector is far from perfect in reconstructing neutrino energies. The optimal migration matrix would be the identity, meaning that the detector reconstructs exactly what energy the initial neutrino had. These migration matrises found in Ref. [41] were used for the simulations of the ESS$\nu$SB experiment.

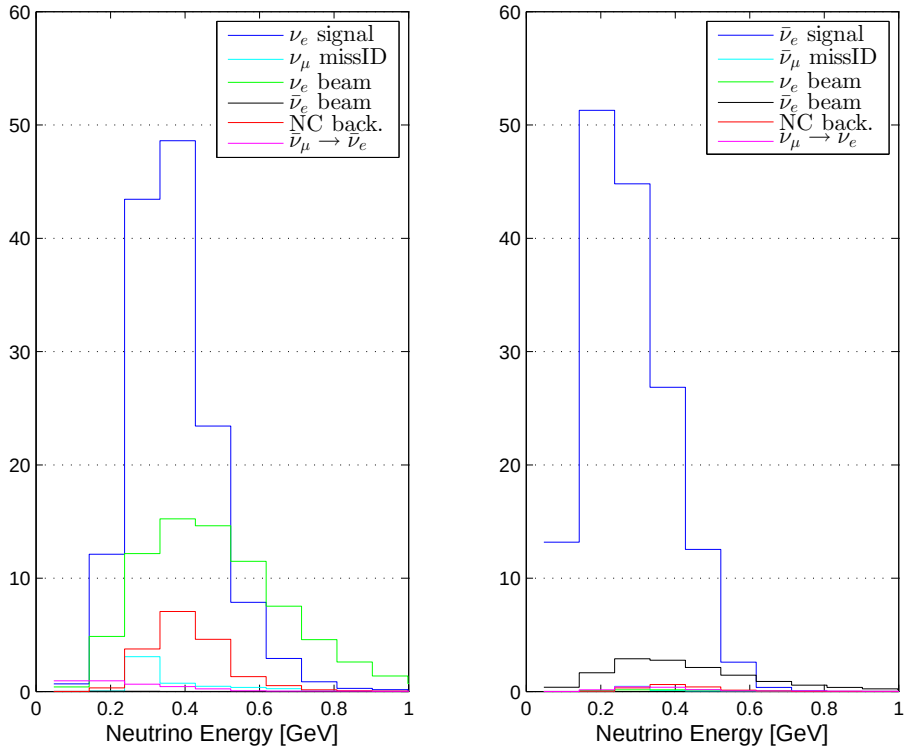


**Figure 6.2:** The left figure contains the energy distribution of neutrinos and the right figure contains the energy distribution of antineutrinos from the ESSνSB. This distribution was compared to the one from Ref. [38] in order to determine the overall normalisation of the neutrino flux.

## 6.2 Oscillation Probability in Vacuum and in Matter

By plotting the oscillation probability in vacuum and compare it to the oscillation probability in matter as in Figure 6.3 it is clear that high statistics experiments will be necessary in order to determine bounds on the parameters. The ESS$\nu$SB baseline can be evaluated by comparing the appearance and disappearance channels. The matter effect at the Garpenberg baseline combines a strong disappearance channel ($\nu_\mu \to \nu_e$) with a significant appearance channel ($\nu_e \to \nu_\mu$) and would subsequently mean that there should be good sensitivity towards matter parameters such as the NSI parameters.

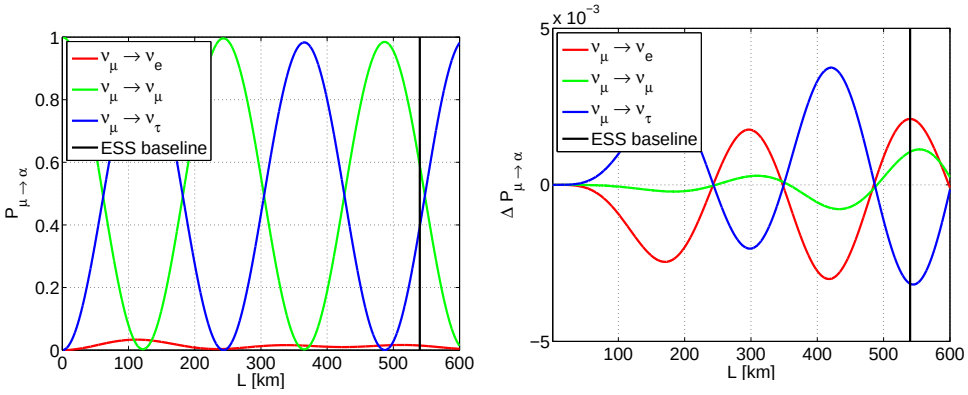


**(a)** Oscillation in vacuum.

**(b)** Oscillation difference.

**Figure 6.3:** Oscillation probabilities ($P_{\mu\to\alpha}$) of an initial muon neutrino in vacuum (left) and probability difference ($\Delta P_{\mu\to\alpha}$) between vacuum and matter (right). The parameter values in Table 6.1 were used. The colour of the line determines what the final flavour of the neutrino is; e (red), $\mu$ (green) or $\tau$ (blue). The black line shows where the preferred ESS$\nu$SB baseline is.

## 6.3 Multidimensional Analysis

### 6.3.1 Standard Interaction Bounds from Simulation

It is of interest to evaluate ESS possibilities to improve current bounds on the parameter $\delta_{CP}$ and to compare bounds on $\theta_{13}$ with the ones produced by the Daya Bay data. In Figure 6.4a the confidence area of the $\theta_{13}$-$\delta_{CP}$ plane is illustrated. It can thus be expected that ESS will be able to determine relatively strict bounds on

these parameters. This is the main purpose of the proposed neutrino experiment and should thus be successful.

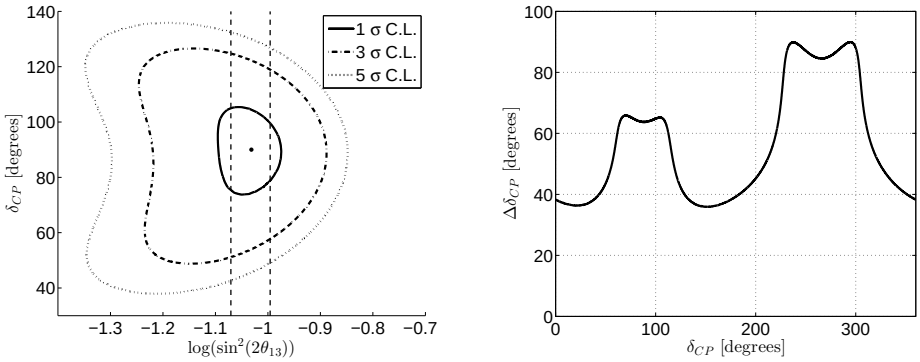


**(a)** Confidence areas. **(b)** Confidence range.

**Figure 6.4:** The left figure contains high C.L. bounds on $\theta_{13}$ and $\delta_{CP}$ from simulation of ESSνSB experiment using the parameter values in Table 6.1. 2 DOF are allowed in the simulation. The dashed lines are the bounds on $\theta_{13}$ from the Daya Bay data. The right figure contains the range of the $3\sigma$ C.L. interval with varying $\delta_{CP}$. The range is calculated for 1 DOF.

A major limitation to $\chi^2$ analysis is that the bounds as a function of a set of data in principle could vary with the true value of the parameter. By then choosing a certain true value for a completely unknown parameter such as $\delta_{CP}$ could then lead to an underestimate of the bounds. The $3\sigma$ C.L. interval range dependence on the true value of the parameter is shown in Figure 6.4b. Here the 90 % C.L. range is calculated for 1 DOF and would subsequently only constitute a rough estimate of the true dependence. If all parameters would have been allowed to vary, the simulation would have become very cumbersome and therefore only the approximation of 1 DOF is used. The simulations were performed with the true value $\delta_{CP} = \pi/2$.

At $1\sigma$ C.L. $\delta_{CP}$ will be within the range between 74 ° and 104 °, at $3\sigma$ C.L. $\delta_{CP}$ will be within the range between 50 ° and 126 °, and at $5\sigma$ C.L. $\delta_{CP}$ will be within the range between 39 ° and 136 °. At $1\sigma$ C.L. $\sin^2(2\theta_{13})$ will be within the range between 0.082 and 0.106, at $3\sigma$ C.L. $\sin^2(2\theta_{13})$ will be within the range between 0.058 and 0.128, and at $5\sigma$ C.L. $\sin^2(2\theta_{13})$ will be within the range between 0.045 and 0.140. This corresponds well to the simulations of Ref. [38]. It should be noted that the Daya Bay experiment has produced better bounds on $\theta_{13}$ than what is expected of ESSνSB. When evaluating Figure 6.4b it can be seen that $\delta_{CP} = 90\,°$ is positioned near a local maximum while the global maximum is one of the maxima surrounding $\delta_{CP} = 270\,°$. This means that the bounds on $\delta_{CP}$ could be weaker if a true value of $\delta_{CP} \approx 270\,°$ was used rather than $\delta_{CP} = \pi/2$.

In order to highlight the problem of multidimensional analysis of parameters Figure 6.5 is plotted. In this figure the 90 % C.L. areas are illustrated for the $\delta_{CP}$-$\theta_{13}$ plane. It can be seen that by performing the analysis on the plane rather than on on the line $\sin^2(2\theta_{13}) = 0.093$ the bounds on $\delta_{CP}$ will increase.

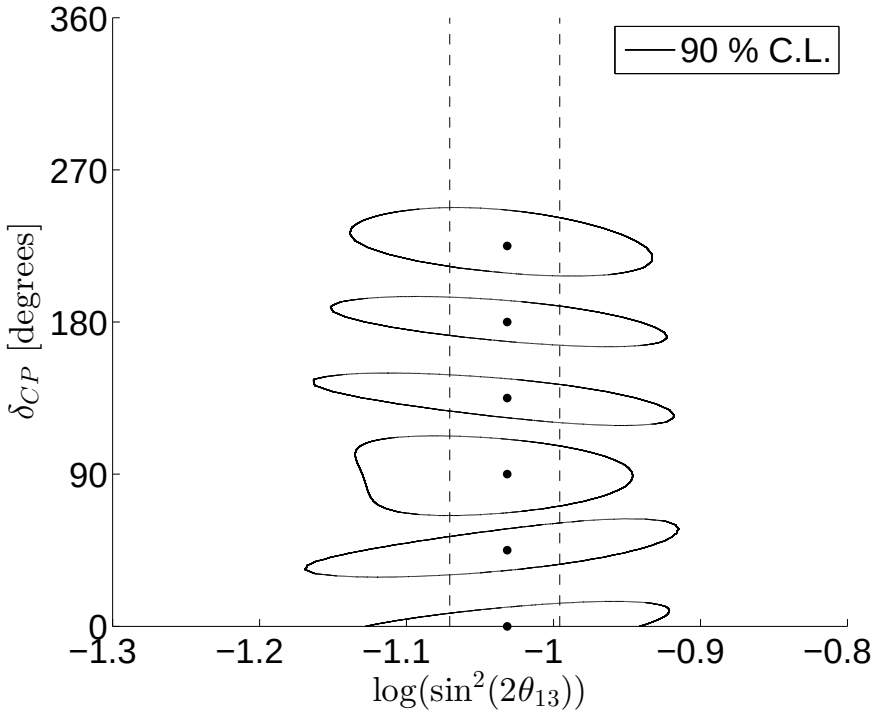


**Figure 6.5:** 90 % C.L. bounds on standard oscillation parameters for different true values of $\delta_{CP}$. True value $\sin^2(2\theta_{13}) = 0.093$ is chosen while $\delta_{CP} = \{0, \pi/4, 2\pi/4, 3\pi/4, 4\pi/4, 5\pi/4\}$. The dashed lines are current bounds from the Daya Bay experiment.

### 6.3.2 NSI Bounds from Simulation

The procedure to evaluate the bounds of each NSI parameter separately from Ref. [17] is reproduced. By considering one non-zero $\varepsilon_{\alpha\beta}$ at the time the bounds can be found from the simulation of the proposed ESS experiment. The bounds were thus calculated using GLoBES with a 90 % C.L. and 1 DOF where the standard parameters were marginalised over the range given in Ref. [11] and the NSI

phases were marginalised over the $2\pi$ range

$$|\varepsilon_{\alpha\beta}| < \begin{pmatrix} 1.8 & 0.22 & 0.26 \\ & 3.7 & 0.085 \\ & & 2.8 \end{pmatrix}. \tag{6.1}$$

These results can then be compared to the ones from Ref. [17]

$$|\varepsilon_{\alpha\beta}| < \begin{pmatrix} 4.2 & 0.33 & 3.0 \\ & 0.068 & 0.33 \\ & & 21 \end{pmatrix}. \tag{6.2}$$

It must however be emphasised that these bounds are found by only considering one non-zero NSI parameter at the time and using the six parameter assumption which was shown to be superfluous in Equation 3.4. The bounds in Equation 6.2 were found using oscillation experiment data as well as solar neutrino data and data on pion and muon decays.

Judging from these bounds ESSνSB should be able to improve the bounds on all NSI parameters except for $\varepsilon_{\mu\mu}$. These improvements are very significant especially in the case of $\varepsilon_{\tau\tau}$ and $\varepsilon_{e\tau}$.

A fundamental issue with this approach is however that the bounds on a certain parameter could depend on the other parameters. This is solved by testing several non-zero parameters simultaneously. The issue is illustrated in the 2-dimensional case in Figure 6.6. In order to determine this relation a hypercube in the parameter space was investigated to determine the true bounds on the NSI parameters.

A problem that arose during the simulation was that there would be no bounds on $\varepsilon_{ee}$, $\varepsilon_{\mu\mu}$ and $\varepsilon_{\tau\tau}$ when the condition $\varepsilon_{ee} = \varepsilon_{\mu\mu} = \varepsilon_{\tau\tau}$ was fulfilled. By then setting $\varepsilon_{\mu\mu} = 0$ as done in Equation 3.5, the realistic bounds on the parameters could be found. As scanning through the complete parameter space is very computationally demanding an efficient Monte Carlo algorithm was used to find the maximal allowed parameter values.

Another limitation of the simulation is inherent in the method itself. When simulating neutrino oscillation data the true value is assumed and bounds are calculated from this point in the parameter space. For example throughout this work all true NSI parameters are assumed to be zero. It is possible that the bounds could be dependent on the true parameter and the dependence is increasing. If the bounds in such a case increased faster than the true value the experiment would not be able to measure the parameter at all. The $3\sigma$ C.L. interval at 1 DOF at varying values for the parameters can be seen in Figure 6.7. The ranges $\Delta\varepsilon_{ee}$, $\Delta\varepsilon_{\tau\tau}$ and $\Delta\varepsilon_{e\mu}$ are clearly decreasing functions of their respective parameter. However, $\Delta\varepsilon_{e\tau}$ and $\Delta\varepsilon_{\mu\tau}$ are not significantly decreasing with the parameter but are on the other hand not increasing significantly either. In the figure $\Delta\varepsilon_{e\tau}$ is increasing slowly at the interval plotted, it is however not fast enough to cause any problems. An interesting observation is that $\Delta\varepsilon_{e\mu}$, $\Delta\varepsilon_{e\tau}$ and $\Delta\varepsilon_{\mu\tau}$ all have an oscillatory effects visible in the plotted ranges. These oscillations are however not caused by any

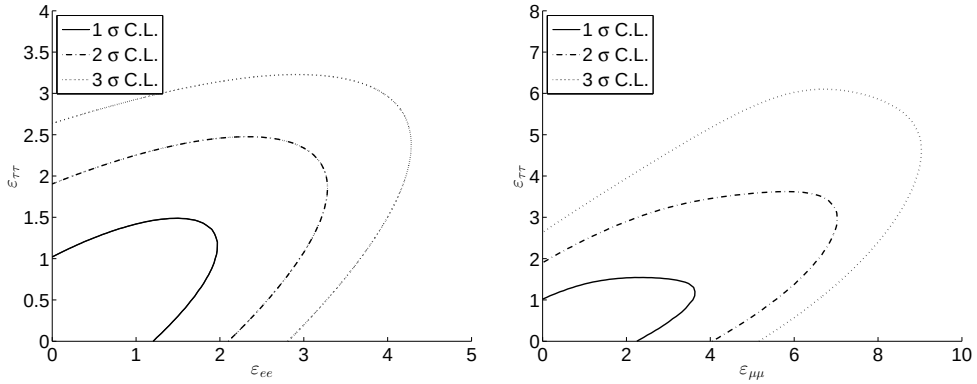


**(a)** $\varepsilon_{ee}$ and $\varepsilon_{\tau\tau}$ **(b)** $\varepsilon_{\mu\mu}$ and $\varepsilon_{\tau\tau}$

**Figure 6.6:** Simulated upper bounds for pairs of non-zero NSI parameters using the parameter values from Table 6.1. It can be noted that increasing the bound of either parameter will result in an increase in the other in these two cases.

attributes of the neutrinos but rather they are caused by the fact that this step in the analyis only considers a single non-zero parameter at the time. If the phase for each of the oscillating parameters would be allowed to vary, the range would not have this property.

The bounds are once again quoted using 90 % C.L. with 1 DOF. Notice that the bounds on $\varepsilon_{\mu\mu}$ is missing due to the separation performed in Equation 3.4. The resulting bounds are given in

$$|\varepsilon_{\alpha\beta}| < \begin{pmatrix} 2.5 & 0.71 & 1.2 \\ & * & 0.53 \\ & & 3.6 \end{pmatrix} \tag{6.3}$$

where the standard parameters were marginalised over the range given in Ref. [11] and the NSI phases were marginalised over the $2\pi$ range.

The choice of which parameter to set to zero is arbitrary but does in principle change the resulting bounds for the other parameters. This is explained simply by making the change of parameters the bounds do no longer relate to the same phenomenon. For example in the parametrisation chosen in this work $\varepsilon_{ee} - \varepsilon_{\mu\mu} \rightarrow \varepsilon'_{ee} \neq \varepsilon_{ee}$. Subsequently the resulting bounds on the diagonal elements in Equation 6.3 cannot be directly compared to the ones in Equation 6.1 or Equation 6.2.

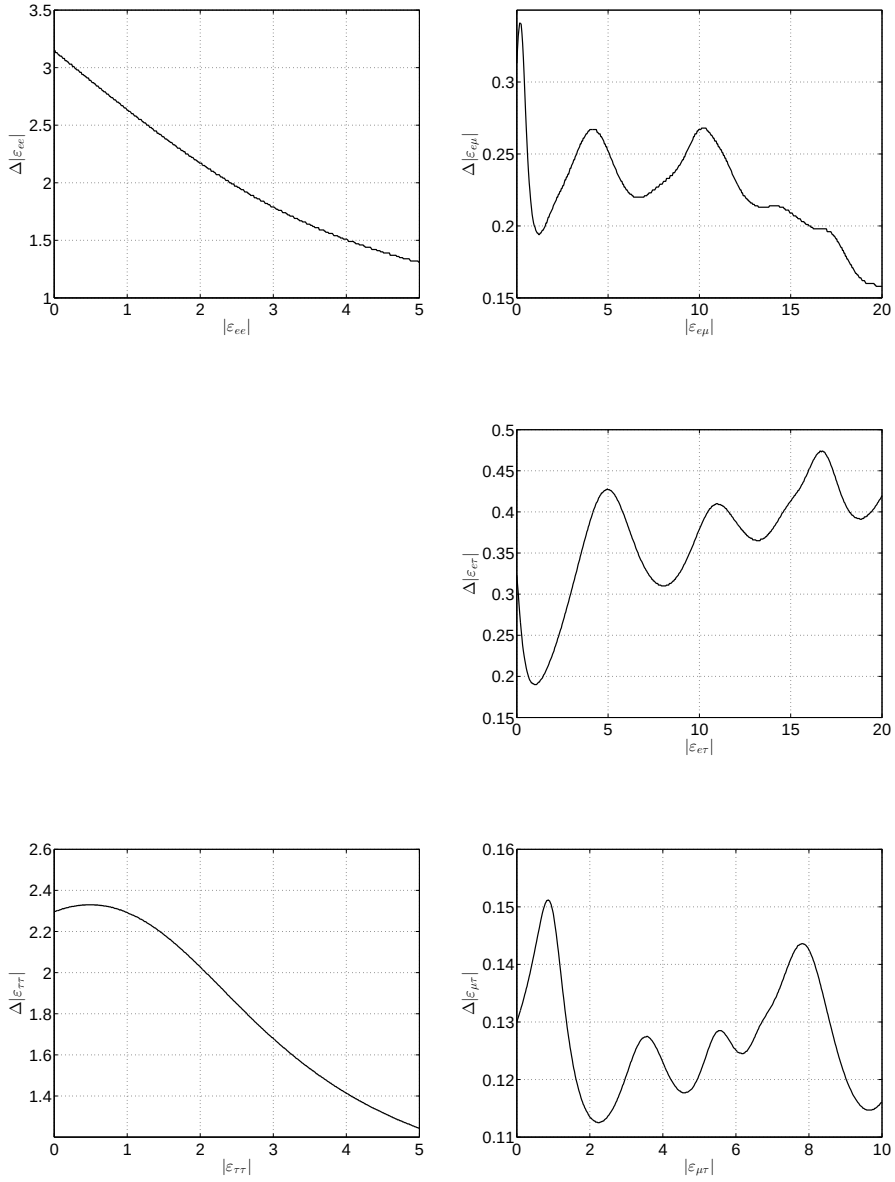


**Figure 6.7:** Length of 90 % C.L. interval $\Delta|\varepsilon_{\alpha\beta}|$ with varying true value of one non-zero NSI parameter $\varepsilon_{\alpha\beta}$ for 1 DOF. Top left: $\varepsilon_{ee}$. Bottom left: $\varepsilon_{\tau\tau}$. Top right: $\varepsilon_{e\mu}$. Middle right: $\varepsilon_{e\tau}$. Bottom right: $\varepsilon_{\mu\tau}$.

### 6.3.3 Numerical Methods

The calculation of upper bounds on the parameters of a numerically defined hyper-ellipse in reasonable time is a non-trivial calculation. The GLoBES software was used to calculate the $\chi^2$ value in any particular point. The transformation

$$\begin{aligned} H &= \log\left(|\chi^2 - \chi_0^2| + \frac{C}{\varepsilon_\alpha + 0.01}\right) \\ H &= -\frac{1}{\log(H+1)} + H. \end{aligned} \tag{6.4}$$

was used to increase the speed at which the function minimizer converges without moving the minimum significantly. Notice however that the minimum actually is moved slightly.

This measure of fitness given in Equation 6.4 between any point in the parameter space and the upper bound of a particular parameter was then minimised by a Monte Carlo algorithm supplied by David Aceituno. The term $|\chi^2 - \chi_0^2|$ ensures that the minimum found by the Monte Carlo algorithm is on the contour defined by the $\chi^2 = \chi_0^2$, where $\chi_0$ is the critical $\chi^2$ value chosen for the particular analysis. As the upper bound of $\varepsilon_\alpha$ is defined by being the largest value of $\varepsilon_\alpha$ on this contour this bound is easily found by adding the term $\frac{10}{\varepsilon_\alpha + 0.01}$. Here $\varepsilon_\alpha$ is strictly positive and thus it is fine to not take the absolute value of this term. Furthermore, $C$ is an arbitrary constant that determines the relative importance of the contour and the particular parameter to be minimised. The value that in general was chosen was $C = 10$ but this had to be adjusted to improve convergence for some parameters. Notice that the position of the numerical minimum is dependent on $C$ and this limits which values that can be used.

By performing the two transformations in Equation 6.4 the algorithm will find a minimum of the new function is positioned slightly higher than the minimum of the inital function. This means that this numerical method will find upper bounds that are slightly more conservative than the actual bounds. Subsequently this discrepancy between the real bound and the calculated bound does not invalidate the bound itself. By taking the logarithm of the sum it is ensured that the values of $H$ are within a reasonable range. By then performing the operation on the second line convergence is improved through making the minimum sharper.

The algorithm used to perform these demanding computations is an evolutionary Monte Carlo algorithm based on Refs. [42–44]. It utilises mutation, crossover and exchange in order to quickly find the minimum of a function depending on an arbitrary set of parameters.

The contour $\chi^2 = \chi_0^2$ could in principle have isolated islands which are separated from the hypervolume close to the true value of the parameter. The algorithm used for the calculations does not take this into consideration and includes the full range between the lower bound and the upper bound of the island.

### 6.3.4 SM Parameter Correction

By introducing the NSI parameters a correction of the observed SM parameters could be necessary. This correction is due to a possible correlation between the SM and the NSI parameters. For example, it is possible that a NSI parameter has a similar effect on the neutrino oscillation as a SM parameter. By allowing a non-zero value for that NSI parameter the related SM parameter might experience a translation of its best fit. This phenomenon is fundamentally the same as that presented above for several simultaneously non-zero NSI parameters. The necessity of this correction is illustrated in Figure 6.8 and is constructed by projecting the $\chi^2$ onto the $\theta_{13} - \varepsilon_{e\tau}$ plane for two DOF. The same relation was found in [40] where a correction of the standard parameters was proposed.

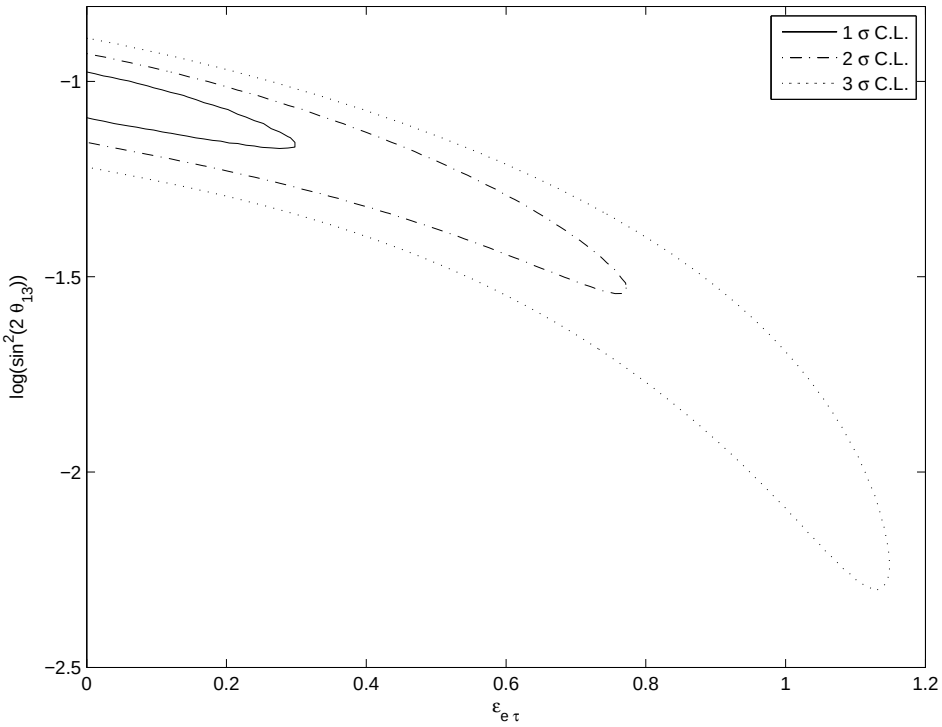


**Figure 6.8:** Illustration of a typical dependence between a SM and a NSI parameter. The simulation was performed with the parameter values that are presented Table 6.1. It is clearly visible that $\theta_{13}$ and $\varepsilon_{e\tau}$ to some extent have the same effect on the oscillation probability. This relation manifests itself in the fact that either of the parameters can be large but not at the same time. The conclusion that can be drawn from such a relationship is that by introducing non-zero NSI parameters the bounds on the SM must be re-evaluated.

## 6.4 CP Asymmetry

Genuine CP violation is observed in vacuum propagation seen in Figure 2.3. The fake matter dependent CP violation is on the other hand observed in Figure 6.9a and it can be compared to vacuum CP asymmetry in Figure 2.3b. It is clear from this comparison that the largest changes when introducing matter are that the asymmetry in $\nu_\mu \to \nu_\tau$ is enhanced and CP asymmetry in $\nu_\mu \to \nu_\mu$ gains a non-zero signal at certain oscillation lengths. By then comparing these asymmetries with that of added moderate NSIs of $|\varepsilon_{\alpha\beta}| = 0.1$ and $\delta_{\alpha\beta} = \pi/2$, the $\nu_\mu \to \nu_\mu$ asymmetry is further enhanced. It should be noted that an observation of a negative CP asymmetry at high cinfidence in the $\nu_\mu \to \nu_\mu$ channel is a significant implication of the existence of NSIs.

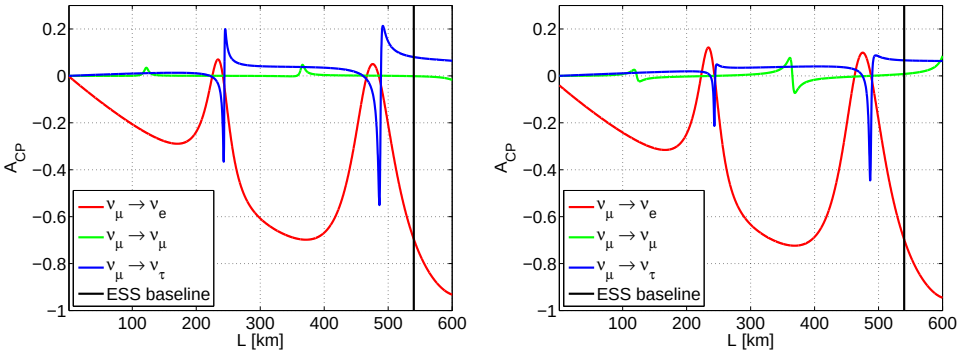


**(a)** CP asymmetry in matter. **(b)** CP asymmetry with NSIs.

**Figure 6.9:** The left figure is a simple recreation of Figure 2.3b with added SM matter interactions. The parameters are set as described in Table 6.1. The right figure has in addition to this a set of small but significant NSIs with values $|\varepsilon_{\alpha\beta}| = 0.1$ and $\delta_{\alpha\beta} = \pi/2$.

# Chapter 7

# Summary and Conclusions

## 7.1 Discussion

### 7.1.1 Theoretical Limitations of Multidimensional Analysis

The first limitation of the simulations of the potential ESS$\nu$SB experiment is the fundamental insensitivity of oscillation experiments to neutral current interactions. These are based on the fundamental insensitivity to all nine NSI parameters. One of these parameters corresponds to the absolute mass scale while two others are Majorana phases leaving oscillation experiments sensitive to six parameters.

The reason why the SM Hamiltonian is parametrised by $\theta_{ij}$, $\Delta m^2_{ij}$ and $\delta_{CP}$ is because a neutrino oscillation experiment is sensitive to the oscillation probabilities and subsequently to these DOF. In principle the effective Hamiltonian including the NSI parameters should be able to be parametrised in a similar way.

The SM and modified NSI together form a 14-dimensional parameter space. A single oscillation experiment is however only sensitive to the six DOF of the effective parametrisation and would subsequently not put very strict bounds on the full set of 14 parameters. Therefore several neutrino oscillation experiments with different matter densities or completely other kinds of experiments are necessary to determine bounds on the full set of parameters.

When introducing NSIs the existing bound on the SM parameters could weaken significantly as NSIs were not considered during the analysis of these parameters. Furthermore as is seen in Figure 6.8 and Ref. [40] there is a significant dependence between $\theta_{13}$ and in particular $\varepsilon_{e\tau}$. In order to fully incorporate NSIs into the existing framework modifications to the values of the standard parameters must be made.

### 7.1.2 Numerical Advantages and Limitations of Multidimensional Analysis

The presented methods of refining the upper bounds of the NSI parameters do not consider the possibility to re-evaluate the known SM parameters when introducing NSIs. For a complete evaluation of these bounds such a consideration must be made where a possible adjustment of the SM parameters is probable. This would require substantially more demanding computations. The Monte Carlo nature of the minimiser does however mean that the time for a computation with 12 or even 15 parameters rather than six parameters would not cause a significant increase in computation time.

This method does however greatly improve on the old method of simply consider one non-zero NSI parameter at the time. By applying the multidimensional analysis in this work strict upper bounds are found rather than the optimistic upper bounds in Ref. [17].

## 7.2 Conclusion

To consider all nine NSI parameters in neutrino oscillation experiments is inappropriate as it generally will result in no bounds at all for the parameters unless additional artificial restrictions are imposed.

The conclusion that can be drawn from the ESS$\nu$SB simulations is that ESS$\nu$SB has good prospects of limiting $\delta_{CP}$. Furthermore it should be able to further limit some of the NSI parameters by imposing better upper bounds.

In the case that NSIs are found to be significant compared to the SM parameters there must be a re-evaluation of the established values of these parameters. Significant NSIs would require a change in the way the SM parameters are found. As such it is of importance to either observe non-zero NSIs or greatly limit them by a strict upper bounds.

# Bibliography


[1] S. Glashow, *Partial-symmetries of weak interactions*, Nuclear Physics **22**, 579 (1961).

[2] F. Englert and R. Rout, *Broken Symmetry and the Mass of Gauge Vector Mesons*, Phys. Rev. Lett. **13**, 321 (1964).

[3] P. Higgs, *Broken Symmetries and the Masses of Gauge Bosons*, Phys. Rev. Lett. **13**, 508 (1964).

[4] S. Weinberg, *A Model of Leptons*, Phys. Rev. Lett. **19**, 1264 (1967).

[5] B. Pontecorvo, *Mesonium and Antimesonium*, Sov. Phys. JETP **6**, 429 (1957).

[6] B. Pontecorvo, *Neutrino Experiments and the Problem of Conservation of Leptonic Charge*, Sov. Phys. JETP **26**, 984 (1968).

[7] R. Davis, D. Harmer and K. Hoffman, *Search for Neutrinos from the Sun*, Phys. Rev. Lett. **20**, 1205 (1968).

[8] Q. Ahmad *et al.*, *Measurement of the Rate of* $\nu_e + d \rightarrow p + p + e^-$ *Interactions Produced by* $^8B$ *Solar Neutrinos at the Sudbury Neutrino Observatory*, Phys. Rev. Lett. **87**, 071301 (2001).

[9] T. Ohlsson, *Status of non-standard neutrino interactions*, Rep. Prog. Phys. **76**, 044201 (2013).

[10] Super-Kamiokande Collaboration, Y. Fukuda *et al.*, *Evidence for Oscillation of Atmospheric Neutrinos*, Phys. Rev. Lett. **81**, 1562 (1998).

[11] Particle Data Group, K. A. Olive *et al.*, *Review of Particle Physics*, Chin. Phys. C **38**, 090001 (2014).

[12] P. Huber, M. Lindner and W. Winter, *Simulation of long-baseline neutrino oscillation experiments with GLoBES*, Comput. Phys. Commun. **167**, 195 (2005).

[13] P. Huber *et al.*, *New features in the simulation of neutrino oscillation experiments with GLoBES 3.0*, Comput. Phys. Commun. **177**, 432 (2007).

[14] L. Wolfenstein, *Neutrino oscillations in matter*, Phys. Rev. D **17**, 2369 (1978).

[15] S. P. Mikheyev and A. Y. Smirnov, *Resonant amplification of $\nu$ oscillations in matter and solar-neutrino spectroscopy*, Il Nuovo Cimento C **9**, 17 (1986).

[16] Daya Bay Collaboration, F. P. An *et al.*, *Observation of electron-antineutrino disappearance at Daya Bay*, Phys. Rev. Lett. **108**, 171803 (2012).

[17] C. Biggio, M. Blennow and E. Fernandez-Martinez, *General bounds on non-standard neutrino interactions*, J. High Energy Phys. **08**, 090 (2009).

[18] A. Giuliani, *Current double beta decay experiments*, Nucl. Phys. Proc. Suppl. **138**, 267 (2005).

[19] Z. Z. Xing and Y. L. Zhou, *Majorana CP-violating phases in neutrino-antineutrino oscillations and other lepton-number-violating processes*, arXiv:1305.5718 [hep-ph] (2013).

[20] M. C. Gonzalez-Garcia *et al.*, *New CP Violation in Neutrino Oscillation*, Phys. Rev. D **64**, 096006 (2001).

[21] C. Bender, D. Brody and H. Jones, *Must a Hamiltonian be Hermitian?*, Am. J. Phys. **71**, 1095 (2003).

[22] S. Antusch *et al.*, *Unitarity of the Leptonic Mixing Matrix*, JHEP **0610**, 084 (2006).

[23] S. Antusch and O. Fischer, *Non-unitarity of the leptonic mixing matrix: Present bounds and future sensitivities*, JHEP **1410**, 096 (2014).

[24] M. Drewes, *The Phenomenology of Right Handed Neutrinos*, Int. J. Mod. Phys. E **22**, 1330019 (2013).

[25] K. Abe *et al.*, *Calibration of the Super-Kamiokande Detector*, Nucl. Instr. Meth. Phys. Res. A **737**, 253 (2014).

[26] IceCube Collaboration, R. Abbasi *et al.*, *Calibration and Characterization of the IceCube Photomultiplier Tube*, Nucl. Instr. Meth. Phys. Res. A **618**, 139 (2010).

[27] KamLAND Collaboration, T. Araki *et al.*, *Measurement of Neutrino Oscillation with KamLAND: Evidence of Spectral Distortion*, Phys. Rev. Lett. **94**, 081801 (2005).

[28] RENO Collaboration, J. K. Ahn *et al.*, *Observation of Reactor Electron Antineutrino Disappearance in the RENO Experiment*, Phys. Rev. Lett. **108**, 191802 (2014).

[29] Y. Abe *et al.*, *First Measurement of $\theta_{13}$ from Delayed Neutron Capture on Hydrogen in the Double Chooz Experiment*, Phys. Lett. B **723**, 66 (2013).

[30] Daya Bay Collaboration, F. P. An *et al.*, *A side-by-side comparison of Daya Bay antineutrino detectors*, Nucl. Instr. Meth. Phys. Res. A **685**, 78 (2012).

[31] MINOS Collaboration, P. Adamson *et al.*, *Measurement of Neutrino Oscillations with the MINOS Detectors in the NuMI Beam*, Phys. Rev. Lett. **101**, 131802 (2008).

[32] T2K Collaboration, K. Abe *et al.*, *Precise Measurement of the Neutrino Mixing Parameter $\theta_{23}$ from Muon Neutrino Disappearance in an Off-axis Beam*, Phys. Rev. Lett. **112**, 181801 (2014).

[33] NO$\nu$A Collaboration, D. S. Ayeres *et al.*, *NOvA Proposal to Build a 30 Kiloton Off-Axis Detector to Study Neutrino Oscillations in the Fermilab NuMI Beamline*, Fermilab-Proposal-0929 .

[34] Y. F. Li, *Overview of the Jiangmen Underground Neutrino Observatory (JUNO)*, International Journal of Modern Physics: Conference Series **31**, 1460300 (2014).

[35] LBNE Collaboration, C. Adams *et al.*, *The Long-Baseline Neutrino Experiment: Exploring Fundamental Symmetries of the Universe*, BNL-101354-2014-JA (2014).

[36] C. Weinheimer, *Direct neutrino mass measurements*, Hyperfine Interactions **215**, 85 (2013).

[37] M. Bogomilov *et al.*, *Neutrino Factory*, Phys. Rev. ST Accel. Beams **17**, 121002 (2014).

[38] E. Baussan *et al.*, *A very intense neutrino super beam experiment for leptonic CP violation discovery based on the European spallation source linac*, Nucl. Phys. B **885**, 127 (2014).

[39] M. Blennow *et al.*, *Exploring Source and Detector Non-Standard Neutrino Interactions at ESS$\nu$SB*, arXiv:1507.02868 [hep-ph] .

[40] D. Meloni, T. Ohlsson and H. Zhang, *Exact and Approximate Formulas for Neutrino Mixing and Oscillations with Non-Standard Interactions*, arXiv:0901.1784 [hep-ph] .

[41] L. Agostino *et al.*, *Study of the performance of a large scale water-Cherenkov detector (MEMPHYS)*, JCAP **01**, 024 (2013).

[42] F. Liang and W. H. Wong, *Evolutionary Monte Carlo: Applications to $C_p$ model sampling and change point problem*, Statistica Sinica **10**, 317 (2000).

[43] G. Goswami and J. S. Liu, *On learning strategies for evolutionary Monte Carlo*, Stat. Comput. **17**, 23 (2007).

[44] Y. Ren, Y. Ding and F. Liang, *Adaptive evolutionary Monte Carlo algorithm for optimization with applications to sensor placement problems*, Stat. Comput. **18**, 375 (2008).